ABSTRACT

Title of dissertation:	LOW-COST PAPER-BASED ASSAYS FOR MULTIPLEXED GENETIC ANALYSIS USING SURFACE ENHANCED RAMAN SPECTROSCOPY
	Eric Peter Hoppmann, Doctor of Philosophy, 2013
Dissertation directed by:	Professor Ian White Department of Bioengineering

In order to improve human health it is critical to develop low-cost sensors for chemical detection and healthcare applications. Low-cost chemical detectors can enable pervasive monitoring to identify health threats. Rapid yet accessible infectious disease diagnostics have the potential to improve patient quality of care, reduce healthcare costs and speed recovery. In both cases, when multiple targets can be detected with a single test (multiplexing), accessibility is improved through lowered costs and simplicity of operation.

In this work we have investigated the practical considerations and applications of ink-jet printed paper surface enhanced Raman spectroscopy (SERS) devices. SERS enables specific simultaneous detection of numerous analytes using a single excitation source and detector. Sensitive detection is demonstrated in several real-world applications. We use a low-cost portable spectrometer for detection, further emphasizing the potential for on-site detection.

These ink-jet printed devices are then used to develop a novel DNA detection assay, in which the multiplexing capabilities of SERS are combined with DNA amplification through polymerase chain reaction (PCR). In this assay, the chromatographic properties of paper are leveraged to perform discrimination *within* the substrate itself. As a test case, this assay is then used to perform duplex detection of the Methicillin-resistant *Staphylococcus aureus* (MRSA) genes *mecA* and *femB*, two genes which confer antibiotic resistance on MRSA. Finally, we explore statistical multiplexing methods to enable this assay to be applied to perform highly-multiplexed detection gene targets (5+), and demonstrate the differentiation of these samples using partial least-squares regression (PLS). By averaging the signal over a region of the SERS substrate, substrate variability was mitigated allowing effective identification and differentiation, even for the complex spectra from highly multiplexed samples which were impossible to visually analyze.

LOW-COST PAPER-BASED ASSAYS FOR MULTIPLEXED GENETIC ANALYSIS USING SURFACE ENHANCED RAMAN SPECTROSCOPY

by

Eric Peter Hoppmann

Dissertation submitted to the Faculty of the Graduate School of the
University of Maryland, College Park in partial fulfillment
of the requirements for the degree of
Doctor of Philosophy
2013

Advisory Committee:
Assistant Professor Ian White, Chair/Advisor
Professor Gregory Payne
Assistant Professor Yu Chen
Professor Philip Bryan
Professor Christopher Davis

Acknowledgments

First and foremost, my heartfelt gratitude to Dr. Ian White for his guidance and patience across the many years of my PhD research, a journey which would have proved entirely less fruitful without the skills and wisdom he imparted on me along the way. Thank you also for giving me flexibility and encouragement to pursue my interests in entrepreneurship even when they proved at odds with being an efficient researcher.

To my committee, thank you for your time, support and helpful discussions. I would be remiss not to acknowledge the financial support the National Science Foundation (ECCS1149850) for my research.

To my colleagues, both past and present: Wei Yu, Soroush Yazdi, I-Jane Chen, Sean Virgile, Jeffry Burke, Kunal Pandit and Stephen Restaino, as well as all of the other members of the White group over the years. You have my sincere thanks for helping support my project and for your part in critiquing and developing the ideas which became this dissertation. A special thanks to Wei Yu for introducing me to paper SERS, and for many helpful discussions along the way.

Finally, a special thanks to my wife, Rebekah, and to my family, for their love and support.

Contents

List of Tables

List of Figures

List of Abbreviations

ALS asymmetric least-squares

BPE 1,2-Di(4-pyridyl)ethylene

CR6G carboxy Rhodamine 6G

CV Cresyl Violet acetate

ELISA enzyme-linked immunosorbent assay

LOOCV leave-one-out cross-validation

MB Methylene Blue

MG Malachite Green oxalate

MRSA Methicillin-resistant *Staphylococcus aureus*

OLS ordinary least-squares regression

PCR principal component regression

PCR polymerase chain reaction

PLS partial least-squares regression

qPCR quantitative real-time polymerase chain reaction

R6G Rhodamine 6G

RMSEP root mean square error of prediction

RRPs Raman reporter probes

SERRS surface enhanced resonance Raman scattering

SERS surface enhanced Raman spectroscopy

SPR surface plasmon resonance

TAMRA tetramethylrhodamine

Chapter 1

Introduction

1.1 Multiplex detection of biological targets

Rapid detection of infectious diseases is critical for improving patient quality

of care, reducing health care costs and speeding recovery. In the USA alone, doctors

report over 20 million cases of infectious-disease-related illnesses annually [6]. Cul-

tures are used for routine diagnosis, but are slow and provide limited information.

Molecular diagnostics (diagnostics which analyze biological markers, often DNA or

proteins) enable accurate and rapid detection, providing results in hours instead of

days [7]. Some tests which target very common biomarkers are low cost and easily

accessible (e.g. pregnancy tests), however these tests are the exception. In general

molecular diagnostics are expensive, requiring samples to be sent to central labs to

be analyzed by highly trained professionals.

The most general purpose and adaptable molecular diagnostic technique, poly-

merase chain reaction (PCR), works through the directed amplification of DNA

targets. However, the cost to run clinical PCR reactions is quite high (typically

$10's to $100 per reaction [8]), and due to the nature of fluorescence (used for PCR

detection), each reaction is typically limited to screening for one or two targets. As

a result, despite the huge potential of PCR, even in wealthy first world countries it

is rarely used for routine screening.

To improve the accessibility of molecular diagnostic tests, specifically PCR, cost and complexity reductions are needed. Two key areas where these reductions can be realized are in sample preparation and in the detection mechanism. When fluorescence transduction is used to detect PCR target amplification, increasing the number of targets being screened for results in a fairly linear increase in costs. This is due to the fact that additional reactions are need for every few targets, necessitating higher volume sample preparation and resulting in additional labor and reagent costs. Additionally, in many clinical scenarios patient samples are of limited volume, making it impossible to run more than one or a few reactions. If an alternate transduction mechanism which enables detection of highly multiplex samples could be used, the number of reactions could be substantially reduced, lowering costs and improving testing accessibility.

1.2 SERS to enable highly multiplex detection in biological assays

Surface enhanced Raman spectroscopy (SERS) is an alternate detection mechanism which relies on the narrow-band nature of a molecule's Raman signature. Raman can be used to uniquely identify molecules, but is a fairly weak effect. By leveraging the plasmonic enhancement of SERS, this effect can be boosted by many orders of magnitude, giving sensitivity comparable to fluorescence [9, 10] coupled with the ability to perform highly multiplex detection. However, a major drawback of SERS is that the substrates needed to provide this enhancement have hitherto been prohibitively expensive.

Herein, we investigate practical considerations and applications of ink-jet printed paper SERS devices, first reported by Yu, et al. [11]. We investigate the effect of substrate support material on sensor performance, the relationship between volume of nanoparticle ink deposited and performance, and demonstrate the application of these sensors to several real-world applications. We then report the development of a novel paper SERS device for analysis of PCR products. Leveraging the chromatographic properties of paper, the sample discimination occurs *within* the paper SERS detection device itself. As a test case for this assay, we perform the duplex detection of the Methicillin-resistant *Staphylococcus aureus* (MRSA) genes *mecA* and *femB*, two genes which confer antibiotic resistance on MRSA. Finally, we investigate statistical methods to enable further increasing the degree of multiplexing of the PCR-SERS assay. Despite the fact that the highly multiplexed samples were impossible to analyze visually due to their complexity, we demonstrate the effective differentiation of these samples using partial least-squares regression (PLS).

Chapter 2

Raman, SERS and molecular diagnostics

Throughout this work, a key assumption is that surface enhanced Raman spectroscopy (SERS) presents a worthwhile alternative detection mechanism to fluorescence. Thus, we begin with an overview of Raman scattering, SERS and SERS substrates. As the chromatographic properties of paper play a key role in the assays presented in Chapters 3 and 4, we then give a brief synopsis of plasmonic paper (SERS on paper). Next, we present various molecular assays for biological analysis, to give context for the assay presented herein, and then explore the application of SERS to biological assays. Finally, a brief introduction to multiplexing and SERS is given.

2.1   Raman and SERS

2.1.1   Raman

When photons interact with a molecule, the vast majority are instantaneously absorbed and emitted with no change in energy. This is termed *Rayleigh scattering*. Rarely, the photons are absorbed and then drop down to an excited vibrational state: this is termed Stokes *Raman scattering*, and is depicted in Figure 2.1. The excited vibrational state is a resonant mode of the underlying molecular structure. The dependence of the Raman scattering on molecular structure is why a Raman

spectrum is unique to a molecule, and is sometimes termed the molecule's "molec-
ular fingerprint". Even more rarely, a photon is already in one of its characteristic
vibrational energy states when it is excited by another incoming photon: in this case,
the emitted photon will be higher energy than the incident photon, and is termed
anti-Stokes Raman scattering. Due to the relative infrequency of this occurrence, it
is rarely used in measurements.
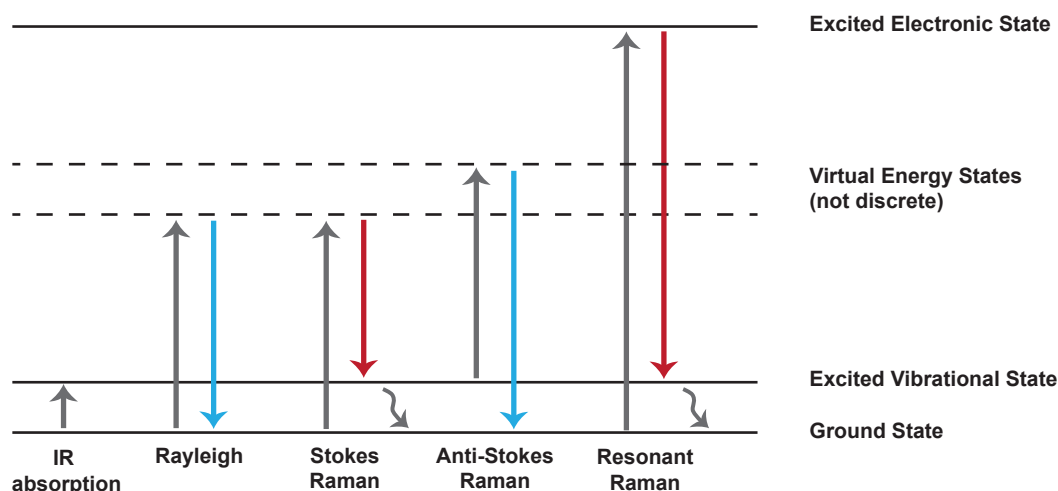
Figure 2.1: Jablonski diagram depicting the processes of absorption
and scattering from a molecule. In the case of Raman scattering, the
molecule is excited to a virtual energy state (non-physical), and then
decays to an excited vibrational state, emitting a photon which
contains information about the underlying structure of the molecule.

Because the molecule is excited to a "virtual energy level" which has no phys-
ical meaning, any frequency of light can be used for Raman scattering. This is a
distinct advantage over techniques such as IR spectroscopy, and wavelengths ranging
all the way from the UV to the IR have been used. While shorter wavelengths pro-
vide much more intense Raman scattering (power $\propto \nu^4$), the inherent fluorescence of

a molecule can often overpower the Raman signature at shorter wavelengths due to the fact that photons rarely undergo Stokes Raman scattering. Thus longer wavelengths at which little fluorescence occurs are preferred. As a result, experiments using Raman are typically done in the mid-visible to IR range (IR having the least fluorescence but the weakest Raman).

One of the key advantages of Raman is the very narrow-band nature of Raman scattering. While fluorescence scattering is frequently spread out over 10's of nm, Raman scattering features are very narrow. As an example the fluorescence emission spectrum of Rhodamine 6G (R6G) is plotted alongside its Raman scattering spectrum (785 nm excitation) in Figure 2.2.
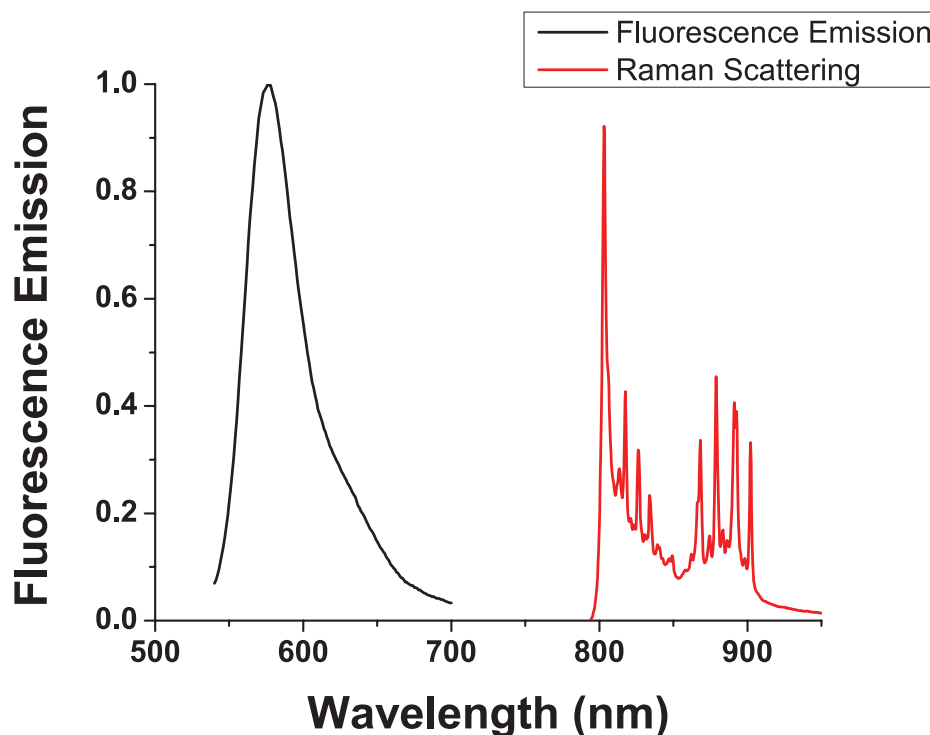
Figure 2.2: Comparison of the broad-band fluorescence emission to the narrow-band Raman scattering spectra of Rhodamine G6 (R6G). Raman scattering spectrum scaled for clarity.

The energy of a Raman scattered photon is given in Equation 2.1, in which the incident photon is represented by the naught subscript and the emitted photon by the one subscript. The term in parentheses is the Raman shift expressed in terms of the wavenumber, and is often reported in units of cm^{-1}. Importantly, Δw is *only* dependent on the difference in energy between the initial and final vibrational states of the molecule and is completely independent of the virtual energy state the molecule was excited to. This gives Raman the powerful property of being independent of the excitation wavelength used for a particular measurement.

$$
\begin{aligned}
E &= h\Delta\nu \\
&= h\nu_\circ - h\nu_1 \\
&= hc\left(\frac{1}{\lambda_\circ} - \frac{1}{\lambda_1}\right) \\
&= hc\Delta w
\end{aligned}
\tag{2.1}
$$

While Raman has several profound advantages over other spectroscopic techniques, it was initially confined to measurement of bulk (pure, concentrated) samples due to the inefficiency of Raman scattering. However, enhancements of many orders of magnitude were made possible with the discovery of SERS, and further enhancements still with the discovery of Resonance SERS.

2.1.2 SERS

On its own, Raman provides a spectral fingerprint which can be used to iden-
tify a molecule based on its unique structure. While this positions Raman as a
compelling analytical technique for bulk materials, it lacks the sensitivity required
for most applications. SERS enables the label-free chemical analysis of Raman to be
performed with similar detection performance to that of fluorescence spectroscopy [9]
and with far superior multiplexing density [4, 12].

Around forty years ago, it was discovered that noble metal nanostructures
boost the Raman signal by many orders of magnitude, for molecules at or near the
surface of the metal [13–16]. This enhancement is provided by both an electromag-
netic enhancement due to surface plasmon resonance (SPR) at the surface [17,18], as
well as a chemical effect [19]. Reports on increasingly sensitive SERS nanostructures
culminated with the demonstration of single molecule detection and identification
about 15 years ago [9, 10, 19, 20].

It is important to note that the SERS enhancement is heavily distance-dependent,
due to the rapid fall off of the SPR electric field. With the radius of a nanoparticle
given by a and a separation of d between the target analyte and the surface, the
SERS enhancement exhibits the following relationship [21]:

$$\text{SERS Enhancement} \propto \left(\frac{1}{a+d}\right)^{12}$$

As a consequence, it is critical that molecules of interest are either very close to
or adsorbed to the nanostructured surface in order to generate a useful enhance-

8

ment [21–23]. An example of the relative electromagnetic SERS enhancement as a function of distance is given in Figure 2.3, with a few common biomolecules given for size reference. For the sake of this example, we assume a spherical nanoparticle with a 60 nm diameter (a = 30), matching the gold nanoparticles we use later. As can be seen, the drop off in SERS enhancement is extremely rapid; when only 2 nm from the surface over 50% of the enhancement has already been sacrificed!
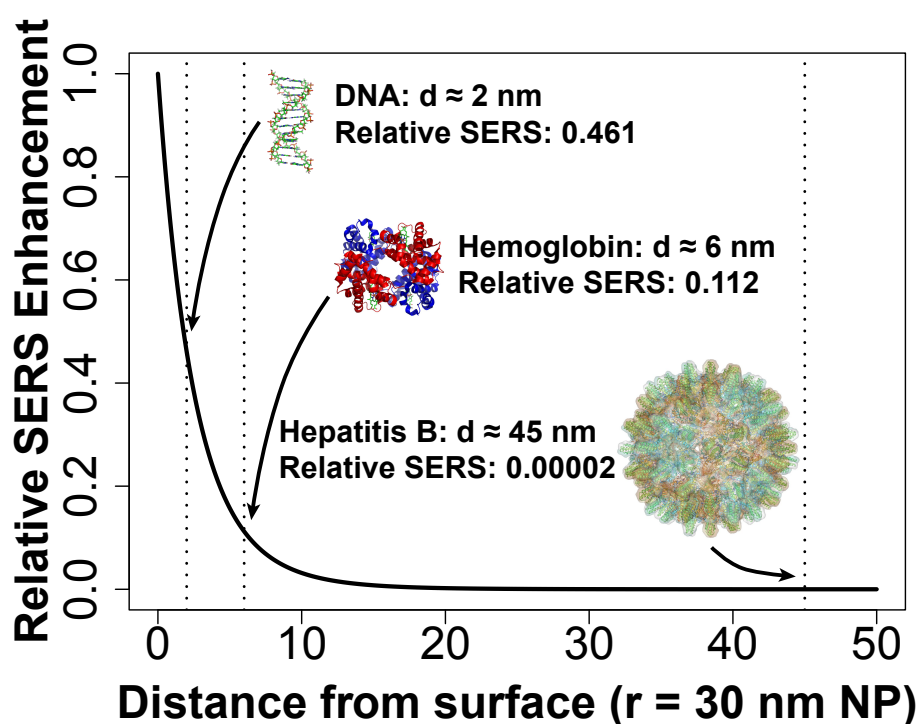
Figure 2.3: Size comparison of common biomolecules vs. the relative electromagnetic SERS enhancement as a function of distance from the surface of a spherical nanoparticle (assuming 60 nm diameter particles)

2.1.3 Resonance SERS (SERRS) for increased sensitivity

While SERS is a highly sensitive technique in its own right, a further optimization is possible through the use of surface enhanced resonance Raman scattering (SERRS). Resonance Raman occurs when a molecule is excited at a wavelength which matches its optical absorption [24–27] (e.g. a fluorescent molecule's excitation wavelength). However, typically the resonance Raman effect is obscured by the fluorescence emission of the molecule, which is orders of magnitude greater than the Raman scattering (unless extremely sophisticated equipment is used which can separate the instantaneous Raman scattering from the slower fluorescence emission). In spite of this, SERS can benefit greatly from the resonance effect since the fluorescence emission is naturally quenched by the metal nanostructure providing the SERS enhancement!

When the excitation wavelength is selected to match the optical absorption of the molecule being detected the scattering cross-section is increased dramatically, improving the detection by a few orders of magnitude [24, 25]. When detecting arbitrary molecules this effect is of limited use, since there is little chance that the molecule will happen to absorb at the excitation wavelength being used. However, in the case of assays employing Raman reporter molecules, SERRS can be put to good use by manually selecting labels which all have high absorption at the assay's excitation wavelength, enabling highly sensitive detection of biomolecules such as DNA [28, 29].

2.1.4 SERS-active nanostructures and substrates

In order for metal nanostructures to generate a SERS enhancement, they must have resonant features (dimensions on the order of the excitation wavelength) and be composed of materials with appropriate dielectric properties and free surface electrons. These appropriately sized resonant features enabled the coupling of the energy of incident light into the oscillations of surface electrons, a phenomenon termed localized surface plasmon resonance. SPR provides the bulk of the SERS enhancement, with the remaining enhancement (one or two orders of magnitude, at most) contributed by the chemical enhancement [22].

The most commonly used materials for SERS are gold and silver, as these metals exhibit resonance in the visible range. While other metals such as copper, nickel, platinum and aluminum can be pressed into service [30], they are typically not used due to their lower absorbances and more damped resonance as compared to gold and silver, though some have use in niche applications such as SERS at UV wavelengths.

In addition to being highly resonant at the excitation wavelength used, the structure of the material at the nanoscale is also important. While a resonant nanosphere provides some SERS enhancement, a cluster of nanospheres provides a dramatically increased enhancement near the junctions of these sphere, so called 'hot spots' [31, 32]. Similar enhancements can be seen near the tips of sharp points, motivating the development of structures such as nanostars and nano-pyrimids. As an example of the enhancements generated at sharp corners and junctions, a

comparison between the electric fields of a single rod and dimer of rods using finite element methods is shown in Figure 2.4A, and an example of the hot spot between two gold cylinders is shown in Figure 2.4B.
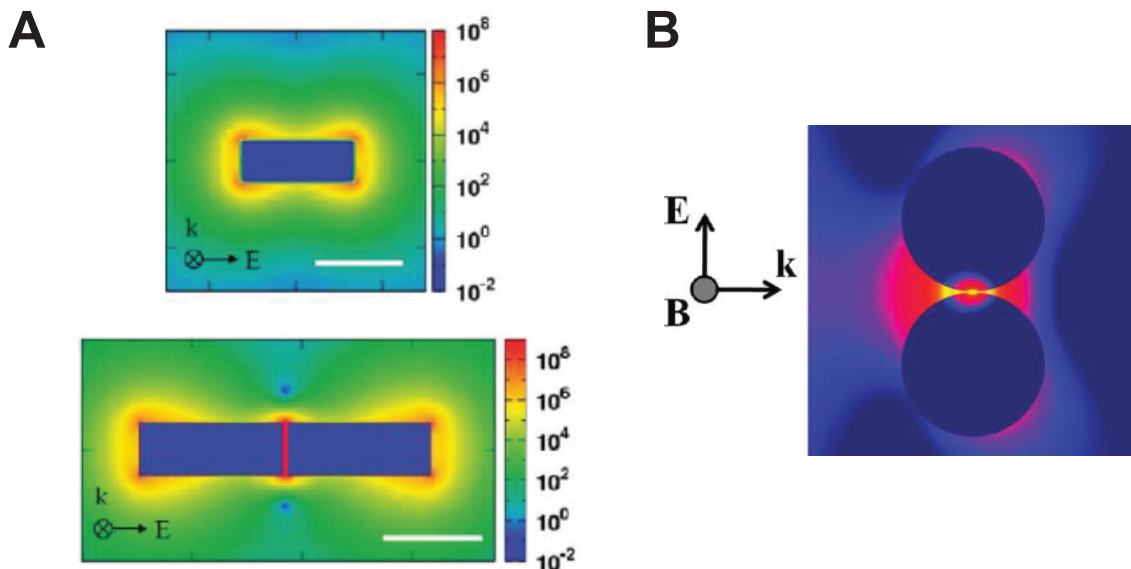
Figure 2.4: (A) Finite element method simlulation results of E_{EM} (the electromagnetic enhancment) generated by a single rod as compared to a dimer of rods. (B) A similar result, except for two spheres. Adapted with permission from McMahon et al. 2012 [2]. Copyright 2012 American Chemical Society.

In practice, SERS-active nanostructures are typically created either in colloidal solutions or through the use of nanofabricated planar substrates. In solution, researchers either create colloids which intrinsically have appropriately sized dimensions to couple with the incident light (e.g. nanorods [33] and nanostars [34]) or through the spontaneous aggregation of nanospheres into resonant aggregates [32]. While effective, solution-based techniques require pipetting and (in the case of aggregation) additional chemistry to be performed at the time of measurement, mak-

ing them difficult to obtain consistent results from. In contrast, nanostructured substrates provide a degree of repeatability and consistency by virtue of being pre-fabricated. In order to use a nanostructured SERS substrate, it is common to deposit a droplet of a liquid sample onto the surface of the substrate and allow it to dry. As the sample dries, the analyte molecules within the sample adsorb onto the nanostructured metal surface, where they will experience the plasmonic and chemical enhancements of SERS.

SERS substrates have been fabricated using a variety of techniques. The initial SERS substrates were formed (accidentally) by electrochemically roughening metal electrodes [13–15], but with increased understanding of the SERS mechanism, fabrication techniques transitioned to more controllable techniques. The substrates yielding the very highest SERS enhancement factors are created through nano-lithography [35–37], which allows for complete control of the nanostructured surface. Another technique yielding very large enhancements is thin film growth [33]. Unfortunately, due to their nature these clean-room fabrication techniques are complex and low-throughput, resulting in extremely expensive substrates.

One strategy to create SERS substrates using more modest resources is to use self-assembly, in which chemical functionality is used to induce the self-directed ordering of nanostructures [38–41]. Another similar class of fabrication is templated assembly, in which a nanoparticles are deposited onto a (frequently sacrificial) templated substrate which guides their ordering [29, 42–44]. While these techniques are often lower cost than nanolithogrpahy, they are still too expensive to be viable chemical analysis tools outside of research labs.

In order for SERS to become a viable solution for low-cost chemical and biomolecule analytics, particularly for use in the field and at the point of sample, a significant shift in the methods for creating SERS substrates is necessary. One promising method which has emerged in recent years is the use of paper as a substrate support for creating low-cost SERS substrates.

2.1.5   Plasmonic paper for low-cost SERS substrates

In order to enable SERS to be used in a variety of everyday applications, the cost of SERS substrates must be dramatically reduced. Current commercial SERS substrates are produced through nanolithography, and cost tens to hundreds of dollars. A shift in fabrication methods is needed to enable SERS to become suitable for its many potential applications.

Recently, a number of promising reports have emerged which demonstrate the fabrication of plasmonic devices using low-cost assembly methods (outside of the clean-room) with paper or other simple membranes as the substrate supports. Using paper as a substrate support offers a number of advantages over the rigid supports required for most other methods. First, the fibers of the paper serve as a low cost template onto which the substrate can be formed. Second, paper is naturally hydrophillic and wicking, simplifying sample application and allowing pump-free movement of liquids as well as chromatographic separations to occur. Finally, the low-cost of paper is a distinct advantage over other substrate supports.

The very first reports of the use of plasmonic nanoparticles deposited onto

paper as SERS substrates came from Vo-Dinh, et al [45, 46]. In this early work, Teflon or polystyrene latex spheres were deposited uniformly onto filter paper, followed by vacuum deposition of silver onto the spheres. These substrates were used to detect various trace organic compounds. Following this, Berthod et al [47–49] reported a different approach to fabricate paper SERS substrates. In their work, silver nanoparitcles were grown *in situ* on the paper surface by soaking the paper in silver nitrate solution and then reducing the silver ions with sodium borohydride.

More recently, research into plasmonic paper substrates has gained momentum as a number of groups have explored fabricating SERS substrates on paper as a viable alternative to nanofabricated and microfabricated substrates. Lee et al [50] and Ngo et al [51] recently explored methods to fabricate plasmonic paper substrates on paper through soaking, and Mehn et al [52] explored the controlled deposition of nanostars through soaking. Looking at alternative deposition techniques, Qu et al explored screen printing for SERS device fabrications [53], while Cheng et al returned to the concept of *in situ* synthesis with a detailed study of the synthesis parameters for plasmonic structures in paper [54]. These substrates achieve a range of enhancement factors and intra-substrate variability, but the fabrication techniques tend to be slow and difficult to scale.

Our group was the first to investigate inkjet printing as a simple and reproducible technique for generating SERS active substrates [11]. In our approach, nanoparticle inks are generated using the simple and scalable method of Lee and Miesel [55] and then deposited onto untreated cellulose filter paper through inkjet printing. In addition to being amenable to mass production, a high degree of relia-

bility and consistency is achieved thanks to the fact that inkjet printing offers very fine control of the rate and volume of ink deposition (typical SERS enhancement variability 5-15% [5]). These substrates have reasonably high enhancement factors around $\approx 2 \times 10^5$ [11, 56], which is similar to other substrates created through semi-random assembly processes, but not as high as those created through nanolithography and templated assembly. As will be explored later, the small variability which is present in these substrates can be mitigated by taking data at multiple locations and averaging (as in Chapters 3 and 5) or by rastering the laser beam over an area at collection time, to achieve this averaging effect in real time (as in Chapter 4).

2.2 Molecular assays for analysis of infectious diseases

The ability to rapidly identify infectious diseases is critical to improving patient quality of care, reducing healthcare costs and speeding recovery. Traditional methods rely on evaluation of the phenotypic characteristics of the target organism, typically through culture, and often in combination with techniques such as antibiotic susceptibility profiling to provide additional specificity [7]. However, these techniques are slow, many times requiring days to conduct. Additionally, limited strain differentiation is possible with these techniques.

Molecular diagnostics enable accurate and rapid detection of infectious diseases. Most commonly molecular diagnostics use the detection of proteins or DNA sequences to inform a diagnosis.

2.2.1 Protein-based molecular assays

Proteins can be used for detection in a number of different ways, including molecular weight based electrophoretic separation [57] and immunoassays. Electrophoresis is relatively simple, but requires trained operators to conduct the assays and interpret the results (which can vary based on an individual lab's protocols) [58], is slow, and is not sensitive to mutations (e.g. those which confer antibiotic resistance).

Immunoassays such as an enzyme-linked immunosorbent assay (ELISA) are well understood, flexible techniques and have some amplification capability since the detection is transduced by the reaction of the captured antibody-enzyme conjugate with the enzyme's substrate resulting in a color change [59] or fluorescence. While fairly powerful, ELISA and other immunoassays are labor intensive (multiple wash and reaction steps) and can require large quantities of reactants.

2.2.2 Nucleic acid-based molecular assays

Nucleic acid-based testing offers excellent specificity, rapid results and is becoming increasingly accessible. With the continuing rapid advances in DNA technology the full genomic sequences for most infectious diseases (and numerous strains) are freely available, and are cost effective to obtain (under $0.10 per million bases in 2013 [60]). As a result, new tests can be developed with relative ease compared to other techniques. With sequence information, DNA probes can be selected, optimized and checked for non-specific hybridization *in silico* at very low cost.

Without amplification, there exist techniques for evaluation of DNA, one of the most prevalent of which is DNA profiling through the use of restriction enzymes. In DNA profiling, restriction enzymes which cleave DNA at sites of certain patterns of bases are added to a sample, and this is followed by a size-based electrophoretic separation which can identify whether the sample matches a reference based on the characteristic patterns obtained [61–63]. While useful, the requirement for large quantities of DNA can be problematic: in many cases, especially for infectious disease detection, large quantities of DNA are simply unavailable. Additionally, these techniques share many of the drawbacks of the protein size-based techniques discussed in Section 2.2.1.

2.2.3 Polymerase chain reaction

For highly specific and sensitive testing, signal amplification is required. Polymerase chain reaction (PCR), in which this amplification occurs through enzymatically increasing the number of copies of target DNA, has emerged as the gold standard nucleic acid detection technique [64]. In its simplest form, PCR works by duplicating a short target DNA region (≈ 100 bases). Short segments of DNA which bracket a region of interest ("primers") are added to the reaction. After heating to denature the target DNA, these primers bind to the target region as the reaction cools, and are subsequently extended to create new copies of the target region by the DNA polymerase (as shown in Figure 2.5). Following many cycles of amplification, a size based separation is performed to identify the presence of amplified target [65].

Genomic DNA
Target region in red

Denaturation
Heat to 95ºC

Annealing
Cooling allows
primers (small arrows)
+ polymerase (green
circles) to bind

Extension
DNA polymerase extends
primers by adding
complimentary bases

Cycle 2
Yields 2^2 = 4 copies

Cycle 3
Yields 2^3 = 8 copies
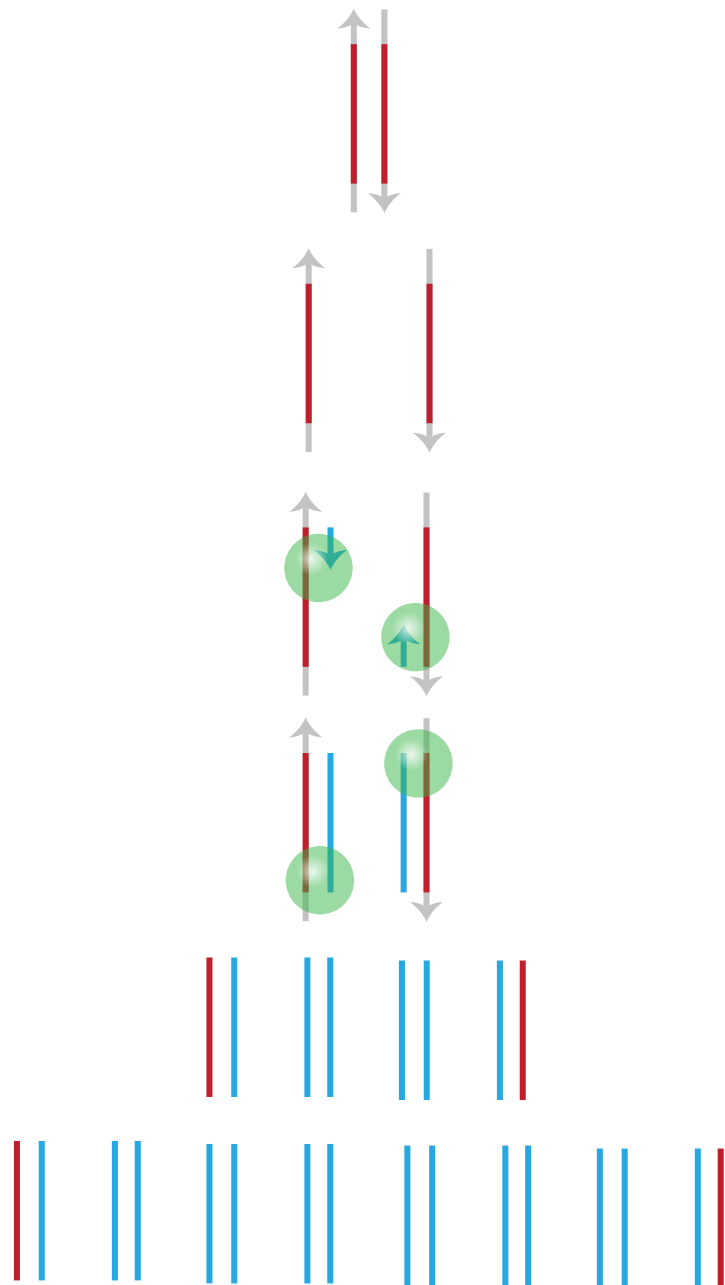
Figure 2.5: Polymerase Chain Reaction (PCR) DNA amplification process. First, the reaction is heated to denature all of the double stranded DNA. Then, as the reaction cools, the primers (short segments bracketing a region of interest) will bind. These short segments of DNA are extended by the polymerase, resulting in duplication of the region of interest. The process is repeated, yielding approximately 2^n copies of the target region per cycle.

While PCR was immediately recognized as a groundbreaking technique, it was only after the development of quantitative real-time PCR (qPCR), in which a dye is added that fluoresces when bound to double stranded DNA thus measuring the increase in DNA during amplification, that PCR became a mainstream analytical technique (Figure 2.6C) [66]. By enabling quantification and eliminating the need to perform an electrophoretic separation following the reaction, labor requirements were dramatically reduced along with a significant increase in assay speed.

The use of an intercalating dye was a great advance, but limits the multiplexing capability of the PCR reaction. To address this drawback (and to increase specificity), two types of qPCR probes have gained popularity: TaqMan probes and molecular beacons. Since these probes can be designed with different fluorophore labels, it is possible to detect and differentiate signals from a few different probes within a single reaction [67, 68]. TaqMan probes (aka hydrolyis probes), have both a fluorophore and a quencher (Figure 2.6A). When the probes are in their native state the fluorescence is quenched through resonance energy transfer. When the target is present, the probe will bind within the primer-bracketed region and will subsequently be hydrolyzed by the *Taq* DNA polymerase during extension, releasing the fluorophore thus allowing it to fluoresce [69]. Molecular beacons operate in a similar manner: in their native state they form a hairpin structure which causes the fluorescence to be quenched (Figure 2.6B). However, they are not hydrolyzed by the polymerase; instead, they are designed such that the distance between the fluorophore and quencher is large enough that they will fluoresce when bound to the target DNA sequence.
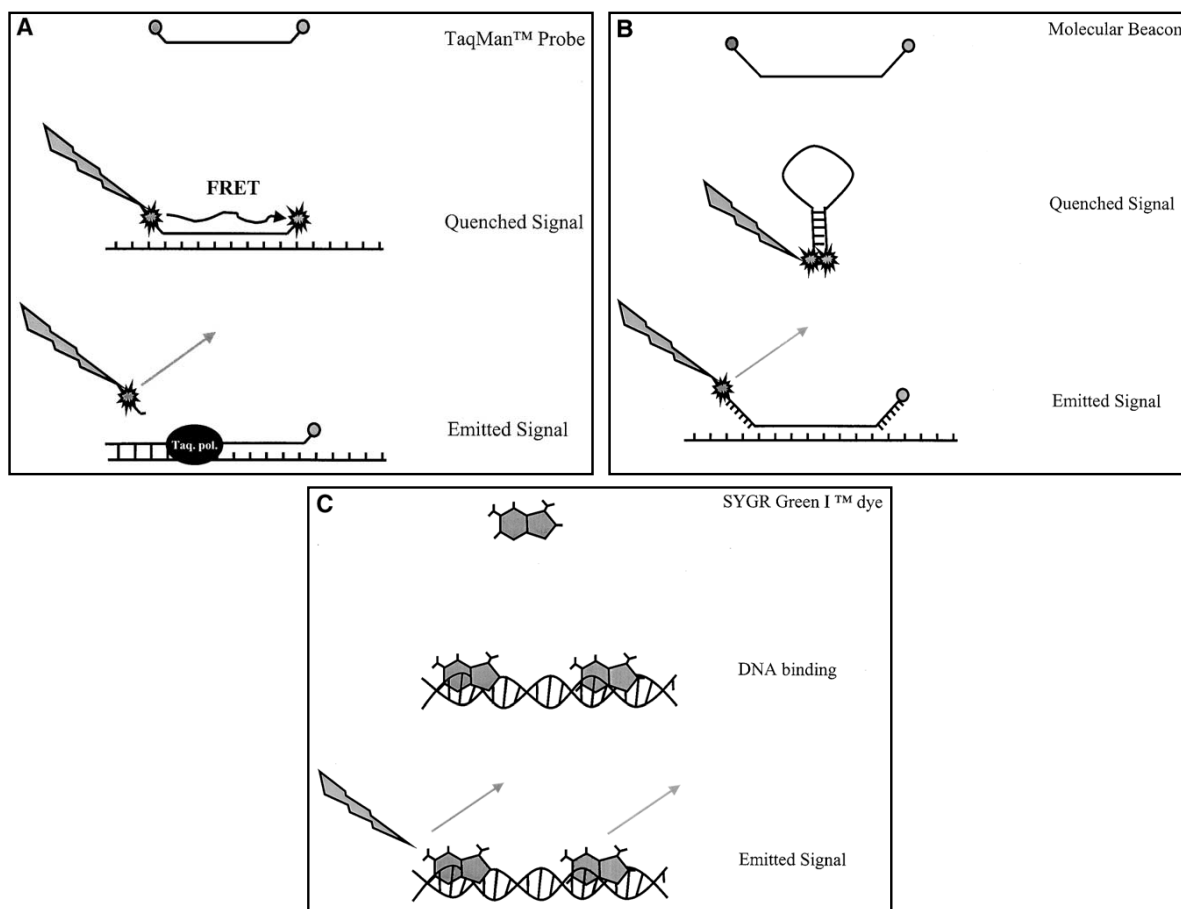
Figure 2.6: (A) A qPCR assay using TaqMan probes. The probe has both a fluorophore and a quencher, and thus emits no fluorescence. However, this probe binds within the region bracketed by primers, and is hydrolyzed during PCR amplification, releasing the fluorophore and enabling detection. (B) A qPCR assay using a molecular beacon. Unlike a TaqMan probe, it is not hydrolyzed during the reaction. Instead, when no target is present it self-hybridizes into a hairpin form, quenching the signal. When the target is present, it will preferentially bind to that and fluoresce, enabling detection. (C) The simplest qPCR assay. A dye is added which fluoresces when bound to double stranded DNA. This allows for direct measurement of the increase in double stranded DNA during fluorescence. While simple and inexpensive, this technique can not be used for multiplex PCR as with A and B. Adapted from Ginzinger et al. 2002, with permission from Elsevier [3].

All of these techniques utilize fluorescence as the transduction mechanism which limits them to one or a few targets per reaction. We present an alternative hydrolysis probe for use with SERS in Chapter 4 which enables much denser multiplexing than fluorescence.

2.3 SERS for biological analysis

SERS is a highly sensitive technique capable of performing label-free detection of small molecules, which exhibit easily identifiable and distinguishable spectral bands. However, for macromolecules such as proteins and DNA the large number of repeating subunits mean that the spectral bands of different macromolecules within the same class are very similar and difficult to distinguish in a reliable and repeatable manner, though some statistical techniques are able to provide limited differentiation in optimal conditions [70]. In order to reliably detect macromolecules it is much more common to employ SERS in labeled assays using Raman reporter probes (RRPs), probes which are labeled with fluorophores or other strong Raman scatterers.

SERS has been utilized in this manner to serve as the detection mechanism in a number of different labeled biological assays, such as immunoassays [71–73] and hybridization assays [29, 74–76]. SERS has also been used to create "SERS tags", in which a SERS active core with Raman reporters is encapsulated within an inert shell which is biologically functionalized [34, 77, 78], enabling Raman to be used as an alternative to fluorescence in biological labeling and imaging.

For highly sensitive and specific detection of DNA targets, it is desirable to perform amplification (as with traditional nucleic acid assays), with SERS providing increased multiplexing capability versus fluorescence. There are a number of reports of combining PCR with SERS [79, 80], however these assays tend to have various drawbacks including negative signal response [81, 82] and poor signal contrast [83].

2.4 Highly multiplex SERS assays

Thanks to the unique narrow-band spectral fingerprints of Raman, it is possible to perofrm highly multiplex detection using only a single laser and filter set [4,84,85]. The first practical demonstration of this capability came from Cao et al., with their demonstration of the use of SERS to specroscopically fingerprint DNA. Their illustrative result is shown in Figure 2.7.

While one can intuit the suitability of SERS for densely multiplexed samples by examining the spectra in Figure 2.7, implementing such multiplexing is somewhat difficult in practice. When viewing one or two spectra simultaneously, one can visually identify the known spectrum or spectra. However, as the multiplexing density exceeds 2 or 3 spectra, it becomes difficult to impossible to manually evaluate the spectra. As a result, even though such highly multiplexed detection represents the single greatest strength of SERS as compared to other signal transduction mechanisms, there are very few reports on highly multiplexed SERS detection [85].

In order to evaluate complex multi-analyte SERS spectra, mathematical analysis techniques are required. Fortunately, this problem is not unique to SERS, and
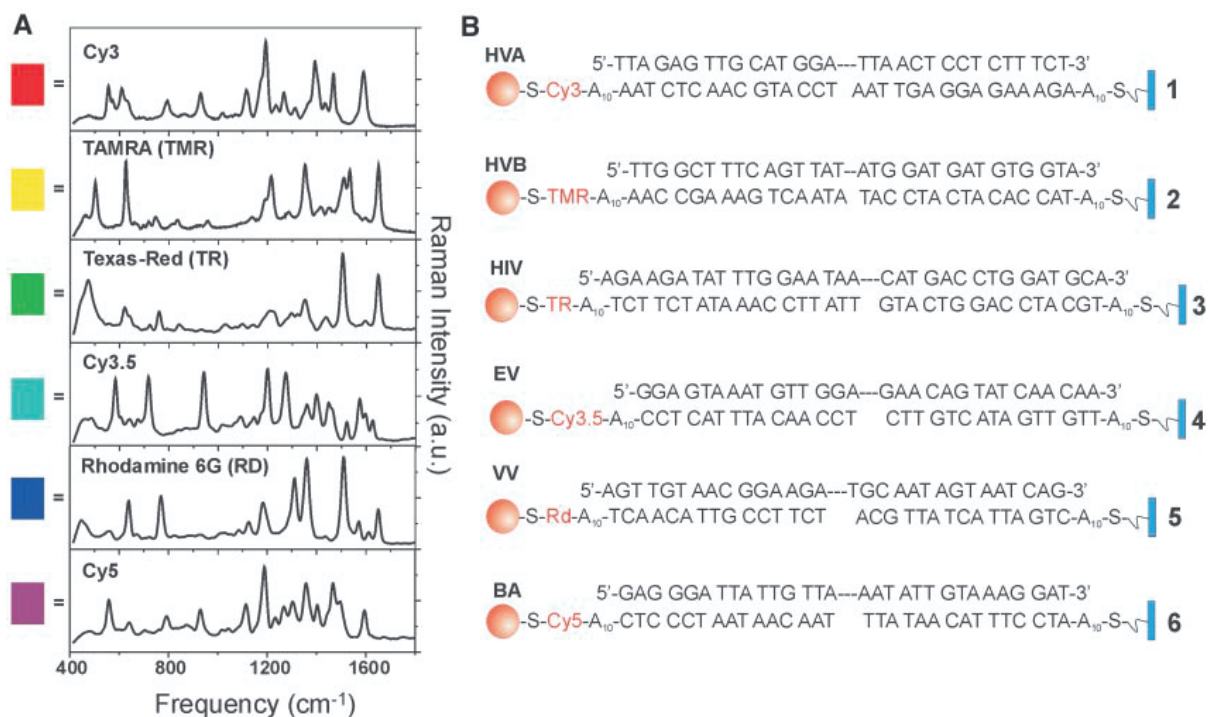
Figure 2.7: Representative Raman spectra from six dye-labeled nanoparticle probes used for multiplexed detection of DANA oligonucleotide targets. Reprinted from Cao et al. 2002, with permission from AAAS [4].

robust techniques have been developed in the field of Chemometrics. The use of such techniques, and their application to SERS is examined in detail in Chapter 5.

2.5 Summary

The high sensitivity and narrow-band nature of SERS makes it an intriguing detection mechanism for a number of different assays. While SERS has been held back by extremely expensive microfabricated substrates or the requirement for the end user to perform colloidal chemistry, low-cost plasmonic paper SERS substrates offer intriguing possibilities. Molecular assays are one area that have the potential to gain the most from SERS as an alternative to fluorescence. In the next chapter, we examine the use of low-cost inkjet-printed SERS devices for analyte identification. We present a duplex DNA detection assay utilizing these substrates in Chapter 4 and then explore the potential to scale this assay to high levels of multiplexing in Chapter 5.

Chapter 3

Highly sensitive and flexible inkjet printed SERS sensors on paper[1]

3.1 Introduction

Today there is significant interest in the development of portable and highly sensitive chemical analysis techniques for use in the field at the point of sample acquisition. Surface enhanced Raman spectroscopy (SERS) has been intensively studied for applications in chemical detection. As discussed in detail in the introduction, SERS offers sensitivity comparable to that of fluorescence spectroscopy [9] while also providing highly specific information about the analyte. This is due to the fact in Raman spectroscopy, photons from a laser source are inelastically scattered at frequencies related to the vibrational energies within the analyte molecule, and thus the measured spectrum uniquely identifies the analyte molecule (generating a "molecular fingerprint"). Although Raman scattering alone is a weak effect, SERS utilizes optical and chemical enhancements from gold or silver nanostructures to provide a tremendous boost to the Raman signal [14–18, 22].

Today, the most common method for performing SERS measurements is to deposit a droplet of a liquid sample onto a rigid silicon or glass substrate that has a nanostructured noble metal surface. When the sample dries, analyte molecules

---

[1]This chapter is adapted from: Eric P. Hoppmann, Wei W. Yu and Ian M. White, *Highly sensitive and flexible inkjet printed SERS sensors on paper*, Methods 63, 219-224, 2013 with permission from Elsevier.

within the sample adsorb onto the nanostructured metal surface, where they will experience the plasmonic and chemical enhancement associated with SERS. The highest SERS enhancement factors are achieved through nanolithography approaches, but are prohibitively expensive to produce. Growth and assembly approaches are less expensive, but suffer from problems of low throughput and high inhomogeneity.

Recently, we reported the fabrication of SERS substrates by inkjet printing silver nanostructures onto paper using a low-cost commercially available desktop piezo-based inkjet printer [11]. These low-cost mass-producible SERS substrates on cellulose paper demonstrate an enhancement factor of about 10^5 to 10^7, which is on par with many of the self assembly and directed assembly techniques. In addition, the paper SERS devices have a number of advantages over rigid SERS substrates. First, liquid samples can be quickly loaded into the paper SERS device by capillary forces (wicking) simply by dipping the paper into the sample. Second, powders and residues, which are incredibly difficult to detect with rigid substrates or microfluidic devices, can be loaded into the paper SERS device by swabbing the inherently flexible device across a wide-area surface of any topology. Finally, analytes loaded into the paper device through dipping or swabbing can be concentrated into a small SERS sensing region by leveraging the concept of lateral flow paper fluidics. Thus, when combining the low fabrication cost of inkjet printed SERS substrates with the fluid handling properties and ease-of-use of paper-based analytics, this new paradigm represents a significant advancement in on-site analytics, and enables SERS to be much more accessible in terms of cost and usability.

Here, we build on the work of Yu et al. [11] as we investigate methods for

27

fabricating paper-based SERS devices explore some potential applications in chemical detection. We detail the methods for generating SERS-active substrates by utilizing a commercial inkjet printer for fabrication, and show how the choice of substrate support material choice and total amount of ink deposited can affect the SERS enhancement. We present SERS spectra for a range of molecules on these ink-jet printed substrates. Detection of the common model analyte 1,2-Di(4-pyridyl)ethylene (BPE) is demonstrated at a concentration as low as 1.8 ppb. The advantage of utilizing the lateral flow concentration capabilities of the paper device are then quantified. Finally, we demonstrate two high-impact applications of the paper SERS devices. First, trace quantities of the fungicide malachite green in water are detected when the sample is loaded simply by dipping the paper SERS device into the water. Second, trace residues of the fungicide thiram are detected by swabbing a surface with a paper SERS device. This collection of results provides an in-depth view of this new low-cost and easy-to-use method for on-site analytical chemistry, and serves as the foundation for the SERS substrate component of the work presented in Chapter 4.

3.2   Materials and Methods

3.2.1   Inkjet printed SERS substrates

Chromatography paper (0.19mm thickness) was purchased from Fisher Scientific. Nitrocellulose membranes were purchased from Bio-Rad Laboratories (Hercules, CA). Chloroauric acid was obtained from Alfa Aesar (Ward Hill, MA). Sodium

citrate and glycerol were obtained from Sigma-Aldrich (St. Louis, MO). Common commercial reagents were of analytical reagent grade.

The gold colloid is synthesized according to the method of Lee and Meisel [55]. Briefly, 80 mg of chloroauric acid is added to 400 mL of DI water (18.2 MΩ) and brought to boil in an Erlenmeyer flask. While stirring rapidly, 80 mg of sodium citrate is added. The color shifts rapidly to a deep purple. The solution is allowed to boil for 20 minutes and then removed from heat.

The gold ink is formed by first centrifuging the gold colloid at $6,000g$ to concentrate the nanoparticles. After removing the supernatant the pellet of nanoparticles is suspended in water to achieve a final concentration factor of 100X. Finally, the ink is created by adding glycerol and ethanol to the concentrated nanoparticles, with a final volume ratio of 5:4:1 of concentrated nanoparticles to glycerol to ethanol. In separate work we have reported the use of silver nanoparticle ink as well [11, 86].

For printing, the ink is injected into refillable printing cartridges. The open source vector graphics editor, Inkscape, is used to define the SERS-active regions for the printed substrates. An inexpensive consumer piezo-based inkjet printer, the Epson Workforce 30, is used to print the SERS-active substrates onto untreated chromatography paper, as previously described [11]. Substrates are printed at least four times to increase the nanoparticle concentration in the paper. The flexibility of ink-jet printing allows arrays of SERS-active regions to be printed in any shape. In Figure 3.1A we show an array of triangular sensors printed for use in dipsticks. After printing the array, devices are cut from the paper to the appropriate size. Various paper SERS devices are displayed in Figure 3.1B-E.
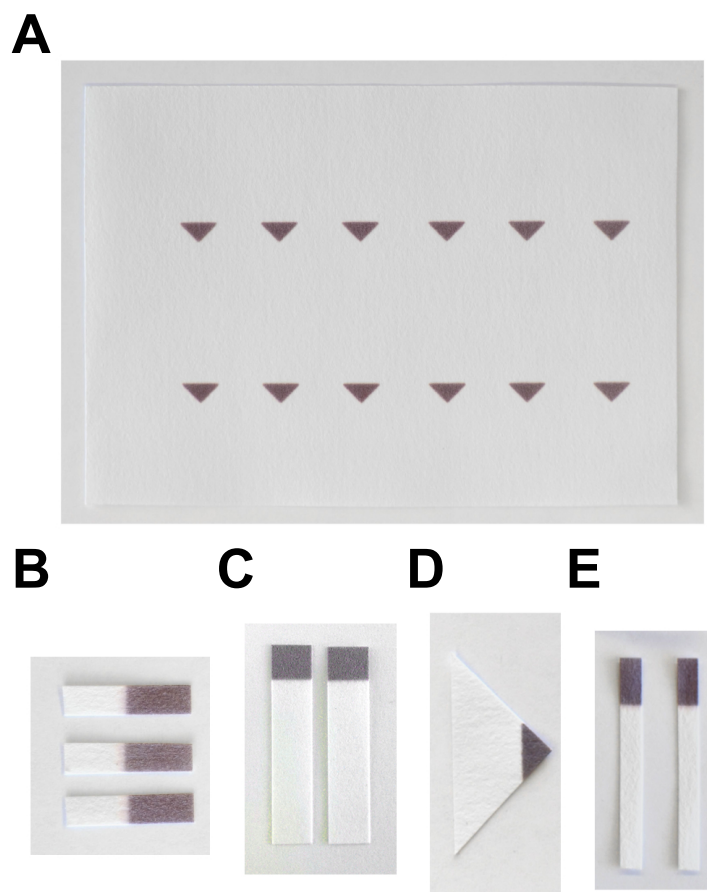
Figure 3.1: (A) A printed array of SERS substrates. Printed arrays of SERS substrates can be cut as demanded by the application, with the goal to create a conformation that most benefits analyte collection, concentration, and detection. (B) Ink-jet printed gold nanoparticles for use as a general SERS substrate. (C) Substrates for use in lateral flow concentration experiments. (D) A substrate with a large wicking region for use as a dipstick. (E) Substrates used as surface swabs.

A scanning electron microscope (SEM) image of a typical ink-jet printed gold substrate is presented in Figure 3.2, showing the clustering of gold nanoparticles in the paper fiber pores. This clustering of nanoparticles is responsible for the high SERS activity of the substrates. While the random aggregation of nanoparticles seen in Figure 3.2 results in local variability of the SERS signal, the large number of nanoparticle clusters captured within the focused region of the fiber optic probe ($\approx$100 μm diameter spot) allows averaging over a multitude of nanoparticle aggregates, lowering variability and enabling quantitative results.

3.2.2   Analyte preparation

1,2-Di(4-pyridyl)ethylene (BPE), malachite green oxalate, and thiram were obtained from Sigma-Aldrich (St. Louis, MO). BPE, malachite green, and thiram were dissolved in ethanol, water, and acetone, respectively; all samples were diluted with water to various concentrations for use as test samples.

3.2.3   SERS measurements

SERS measurements were performed using a 785 nm laser (17 mW) for excitation, a QE65000 (Ocean Optics) portable spectrometer for detection, and a fiber optic probe (InPhotonics) for delivery of laser light and collection of scattered photons (Figure 3.3). The 785 nm wavelength was chosen due to the low cost and portability of 785 nm laser diodes, as well as the reduction in background fluorescence gained by operating at long wavelengths. An integration time of one second was used for all
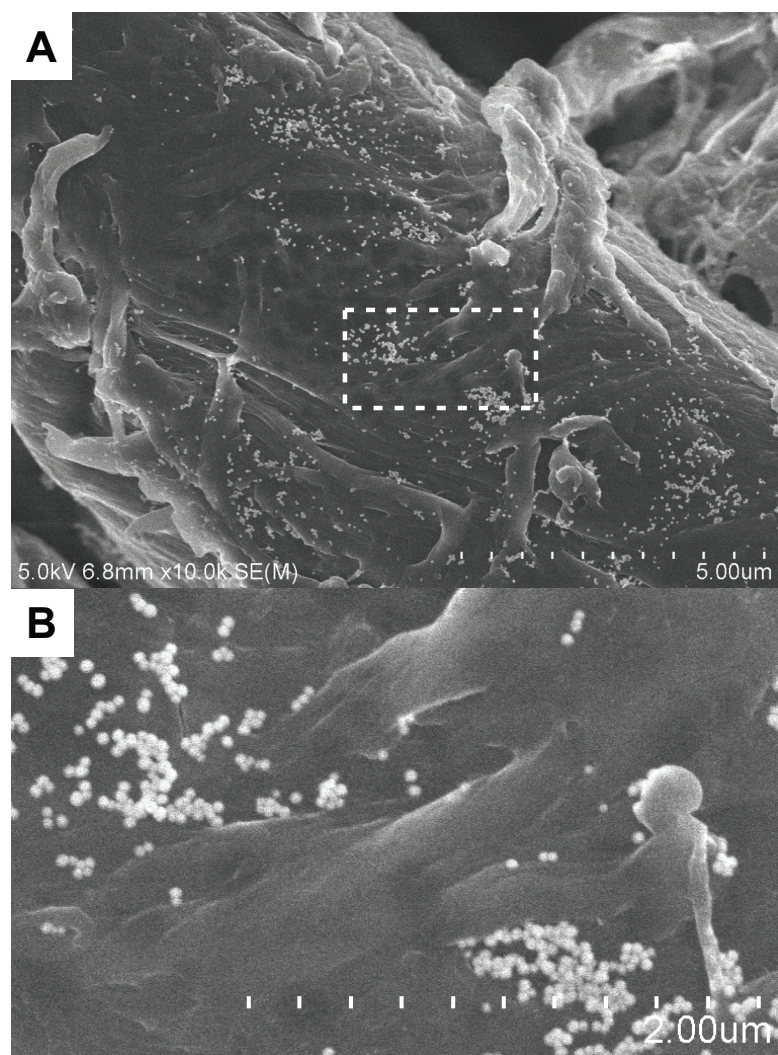
Figure 3.2: (A) Scanning electron micrograph of a printed gold nanoparticle region on cellulose paper. (B) Clustered gold nanoparticles on the cellulose fiber (from box in (A))

measurements; signals represent the average of three measurements. This averaging step reduces the random background noise contributed by the detector; we found that averaging across three signals was sufficient to reduce a large fraction of the noise without contributing a significant amount of acquisition time. Using a linear translation stage the fiber probe was focused to maximize signal intensity for each sample before data acquisition.

For each measurement, the spectrometer records a spectrum in which the Raman scattered photons are represented by spectral peaks; the collection of peaks are used to identify the analyte. To quantify and analyze these results for sensing purposes, the following steps are taken. The magnitude (in photon counts) of the most prominent peak in the spectrum (e.g., 1207 cm^{-1} for BPE) is determined by taking the difference between the value at the peak and the value at the nearest local minimum. This spectral "peak height" is considered as the signal intensity. To determine the detection limit for BPE, the signal intensity is plotted against concentration and a linear fit of the 3 lowest concentration data points is performed; the concentration at which this fit is equal to 3 standard deviations of the mean intensity (1207 cm^{-1}) of the blank samples is considered to be the detection limit.

In order to obtain reference spectra of the three analytes malachite green, thiram, and BPE, 2 μL droplets of each were applied to 4×8 mm sections of printed gold substrates (Figure 3.1B, total device size 4×15 mm). Substrates were then dried in ambient conditions for 20 minutes and SERS measurements were taken as above. Each substrate was interrogated at six or more locations uniformly spread across the entire SERS active region; these spectra were averaged before plotting. SERS

data from typical devices have relative standard deviations, $|\sigma/\mu|$, that range from 15% at low analyte concentrations to 5% at high analyte concentration. Cellulose paper and nitrocellulose membranes were both utilized to demonstrate the concept.
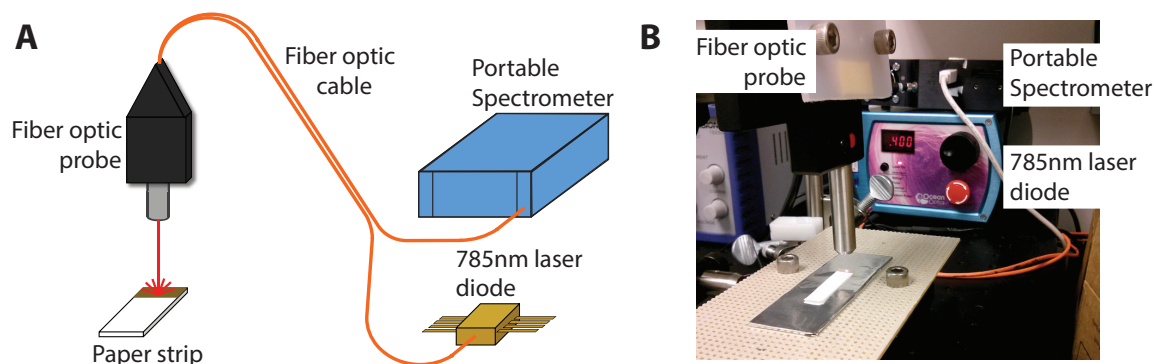
Figure 3.3: (A) Schematic of SERS detection using a small and portable spectroscopic setup. A fiber optic probe is used for delivery of laser light and collection of scattered photons, which are delivered to a portable spectrometer. (B) Photograph of actual setup.

3.2.4   Lateral flow concentration

For the lateral flow concentration experiments, 30 μL of 10 ppb BPE was applied uniformly to the entire 25×5 mm paper strip (Figure 3.1C); this volume had been pre-determined to saturate the paper strip. After drying for 20 minutes in ambient conditions, baseline SERS measurements were taken across the 4×5 mm gold region at the top of the paper strip. The bare paper end (no gold) of the dipstick was then dipped into methanol for 2 minutes, allowing the loaded sample to concentrate in the gold region at the top of the paper strip. Methanol was selected as the mobile phase for its high vapor pressure (faster concentration) and for the high solubility of BPE in the solvent. After the paper strip dried, the SERS signal

was measured.

3.2.5 Dipsticks

An isosceles triangle with a 4 mm high SERS active region at one tip was used as a dipstick (Figure 3.1D, 28 mm base and two 20 mm sides). The gold-printed region of the dipstick was dipped into a vial containing the sample of interest (in water), allowing the dipsticks to soak up liquid for either 1 or 30 seconds. After drying, the SERS signal was measured at 9 points forming a grid across the SERS-active region and averaged. Averaging across a relatively large number of points is necessary for two reasons: (i) SERS is infamous for signal variability when nanoparticle aggregates are used, and (ii) the analyte molecules are not uniformly distributed throughout the sensing region, a result of the location dependent rate of sample collection and concentration. This averaging methodology enables a representative picture of analyte collection and concentration even with these high-variability factors (0.33 coefficient of variation).

3.2.6 Swabs

For the swab experiments, strips of paper with 4×8 mm SERS-active regions at one end were used (Figure 3.1E). The paper was folded 90 degrees where the gold region ends, and the bare end (no gold) was used to hold the swab while wiping the SERS-active region across the surface. The analyte (thiram in acetone) was applied to a clean glass slide with an approximate surface density of 1.25 ng/mm^2.

After allowing the slide to dry, the entire swab was dipped in acetone and then carefully wiped across the entire sample-containing region of the slide twice. After drying, SERS measurements were taken across the entire SERS-active region (n=9 in 3×3 grid) and averaged to reduce variability due to uneven sample collection. A background spectrum from an unused SERS substrate was recorded as a reference and subtracted from the recorded data.

3.3 Results and Discussion

3.3.1 Identification of chemicals with paper SERS

To demonstrate that the SERS-active paper devices can be used for the spectroscopic identification of chemicals, sample droplets (2 μL) were deposited onto the region of the cellulose strips onto which nanoparticles has already been printed. Three model analytes were utilized: malachite green (1 ppm), thiram (240 ppm), and BPE (180 ppb). The respective spectrum for each analyte is presented in Figure 3.4 (the upper black trace in each figure). The unique landscape of Raman peaks within each spectrum can be used to identify each molecule.

Results are also shown for the same three model analytes deposited on nanoparticle-functionalized nitrocellulose, rather than cellulose paper (the lower red traces in Figure 3.4). The SERS-active nitrocellulose substrates yield strong Raman signals for BPE and thiram; however, for malachite green, the signal is significantly lower as compared to SERS-active cellulose paper. This collection of results indicates that in general, inkjet-printed SERS-active nitrocellulose membranes can also be used
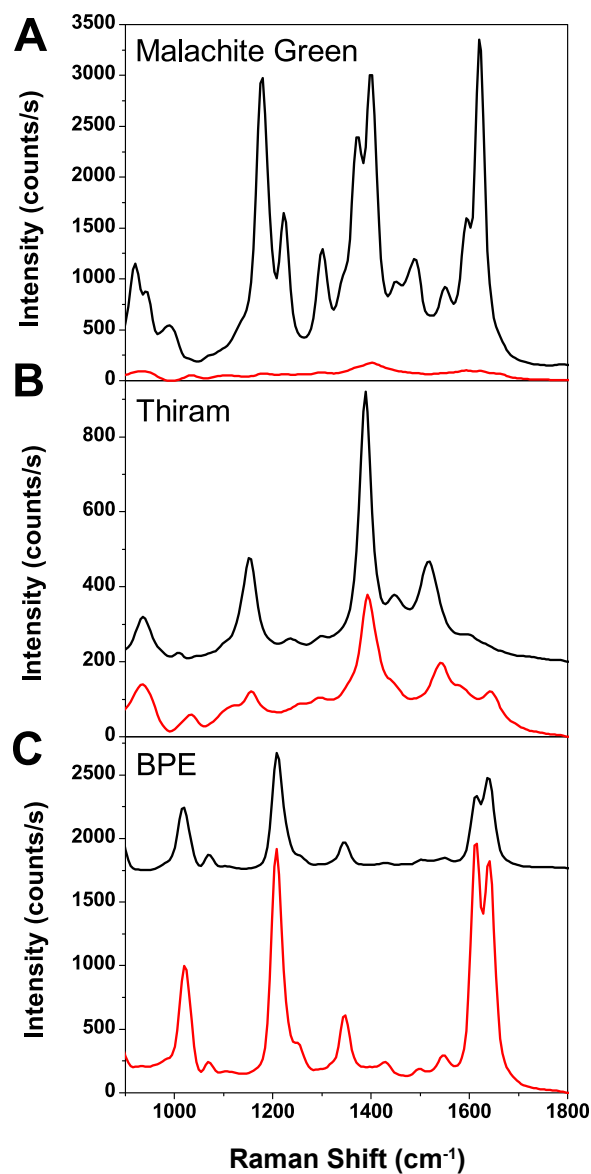
Figure 3.4: Representative spectra of target analytes. In each figure, the top black trace is acquired using gold on cellulose substrates, while the lower red trace is acquired with gold on nitrocellulose substrates. (A) SERS signal from 2μL 1ppm malachite green. (B) SERS from 2μL 240ppm thiram. (C) SERS from 2μL 182ppb BPE.

for chemical identification, but some molecules, such as malachite green, may have strong interactions with the nitrocellulose that inhibit adsorption onto the metal nanoparticles. Nevertheless, this demonstrates the viability of using alternate paper types for ink-jet printed SERS substrates, which provides an excellent avenue for additional assay optimization.
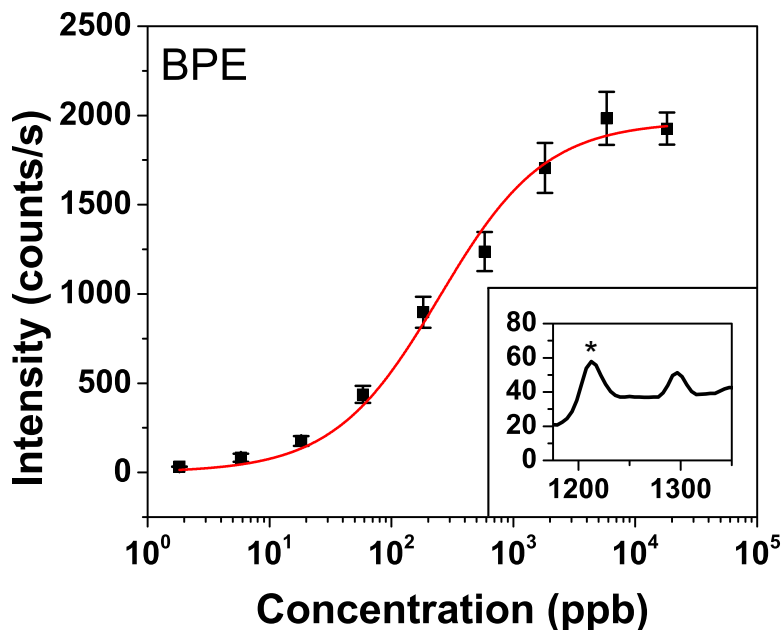
Figure 3.5: BPE SERS signal intensity vs. concentration. Signal intensity is measured at 1207 cm^{-1}. Data is fitted using the Langmuir isotherm. Error bars represent the standard deviation of the 1207 cm^{-1} peak height, as measured at 6 locations distributed across the SERS active region. Inset: recorded signal for 1.8 ppb BPE. Asterisk marks the 1207 cm^{-1} peak.

To further quantify the performance of the paper-based SERS devices, SERS measurements for BPE were repeated over a range of concentrations. The magnitude of the 1207 cm^{-1} Raman peak is plotted versus BPE concentration in Figure 3.5. The data points are fitted with a Langmuir isotherm with an R^2 of 0.99, which demonstrates the repeatability of our methodology. The Langmuir isotherm de-

scribes the chemical equilibrium of the interaction between BPE and the substrate, and is based on the assumption that there exist a fixed number of potential surface binding sites. This result implies that these paper-based SERS sensors can perform quantitative detection of chemicals. The detection of BPE is shown at the low concentration of 1.8 ppb (Figure 3.5, inset). The limit of detection was calculated to be 1.1 ppb (12 femtomoles), which compares well with other substrates produced through directed and self-assembly, though it is not as at the same level as some reports that use sophisticated nanofabrication techniques [87–89].
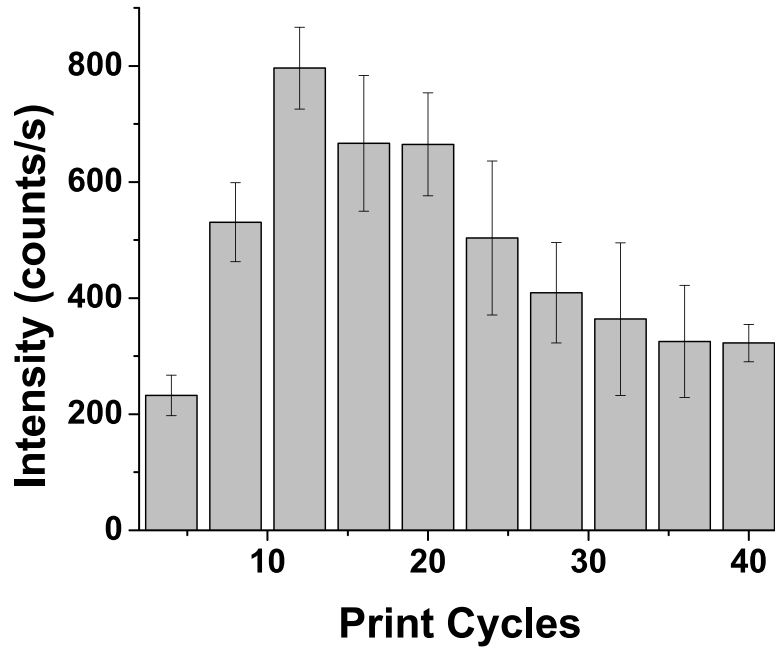
Figure 3.6: SERS signal intensity for BPE at 1207cm^{-1} vs. number of print cycles. Error bars represent the standard deviation of the 1207cm^{-1} peak height, as measured at 6 locations distributed across the SERS active region.

3.3.2 Effect of number of print cycles on performance

The amount of gold nanoparticle ink deposited on the cellulose substrate has a direct effect on the detection sensitivity of the substrate, and is thus an important parameter to optimize when fabricating paper-based SERS substrates. To assess the impact of the number of print cycles, 2 μL droplets of 1 ppm BPE (11 pmol) were applied to inkjet-printed substrates fabricated with varying numbers of print cycles. As expected, the data in Figure 3.6 show a trend of increasing signal intensity with increasing print cycles, which peaks at 12 print cycles. Beyond 12 cycles, however, the measured signal begins to decline with additional print cycles. This biphasic trend appears to imply that an increasing number of nanoparticle clusters initially improves the signal, but after 12 cycles this effect is countered by interference due to excess amounts of other components in the ink. Naturally, this optimal cycle number will vary for different printers and different ink formulations.

3.3.3 Lateral flow concentration

The data in Figure 3.5 demonstrates that the paper-based SERS devices can be used for the quantitative detection of trace levels of analyte in solution. Additionally, as described above, paper-based SERS devices offer a unique advantage over rigid SERS substrates; after loading a relatively large volume of liquid sample into the paper device, the analyte molecules within the paper can be concentrated into a small sensing region through lateral flow concentration. To illustrate the advantage of the lateral flow concentration step, 30 μL of BPE in water (10 ppb) was uniformly

loaded into a paper strip with a pipette; Au nanoparticles had been printed at one end of the to define the sensing region. After drying the paper, the strip was dipped into methanol such that the methanol wicked into the paper and carried the analyte molecules up to the SERS-active tip of the lateral flow dipstick.
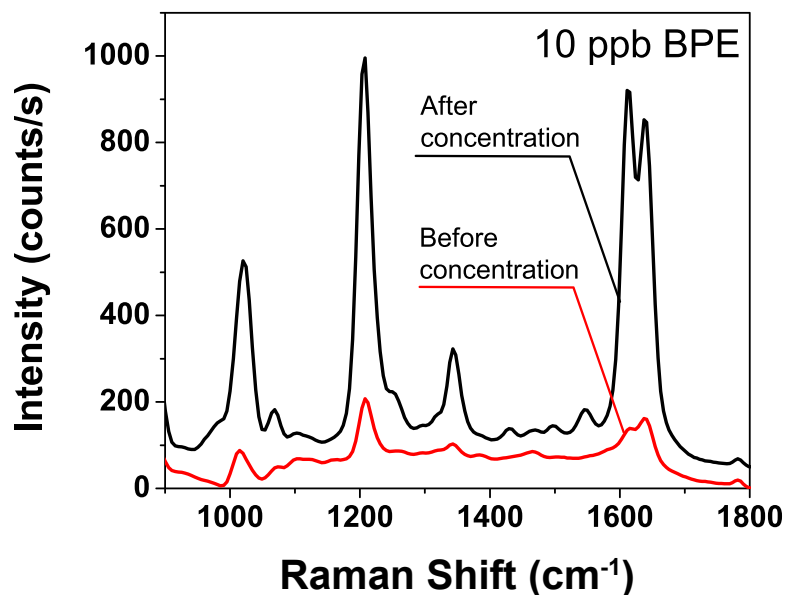
Figure 3.7: Comparison of SERS intensity before and after lateral flow concentration.

The BPE spectra before and after lateral flow concentration are presented in Figure 3.7. The signal magnitude increases by nearly an order of magnitude due to the concentration of BPE molecules into the sensing region upon dipping the paper strip into the methanol mobile phase. Thus, while the inkjet-fabricated SERS substrate was shown to be highly sensitive, the inherent concentration capabilities of the paper can be leveraged to provide a significant improvement in the detection limit.

3.3.4 Application: detection of fungicide in water

Malachite green is a highly effective fungicide used in fish farms by the aquaculture industry. However, malachite green and its metabolite leucomalachite green are suspected mutagens [90], and are stored in fish tissue for extended periods of time [91]. As a result, malachite green is banned in many countries and thus its use must be monitored. To analyze a water sample for malachite green with a rigid SERS substrate, two approaches could be utilized: (i) a droplet ($\approx 2 \ \mu$L) could be spotted onto the substrate and dried, or (ii) the substrate could be submerged and soaked in the water sample such that target analytes may diffuse to the substrate and possibly adsorb. In contrast, with paper-based SERS sensors, the paper strip is simply dipped into the water sample, allowing the sample to be wicked into the sensing region. This ease of use is particularly well suited for the detection of pesticides and other toxins in environmental water samples at the point of sample collection.

To illustrate this application, a paper-based SERS device was dipped into malachite green (1 ppb in water). In this case, the nanoparticle-printed region of the paper strip is submerged into the sample, while the rest of the paper strip acts as a reservoir to wick in the water; as the water is drawn into the paper strip, malachite green molecules pass through the nanoparticle-printed area. The spectra recorded after a 1-second dip and a 30-second dip are shown in Figure 3.8. Even after only a 1-second dip, the spectral signature of 1 ppb malachite green is clearly visible. As expected, by leaving the paper in the water sample for additional time, malachite green is continually drawn into the SERS active region, which results in

an increased signal magnitude. The rate at which the analyte is drawn into the region - and thus the potential enhancement due to additional soaking time - will depend on the size of the paper reservoir. We anticipate that the paper size and dip time can be optimized based on the particular field use application and the required detection performance.
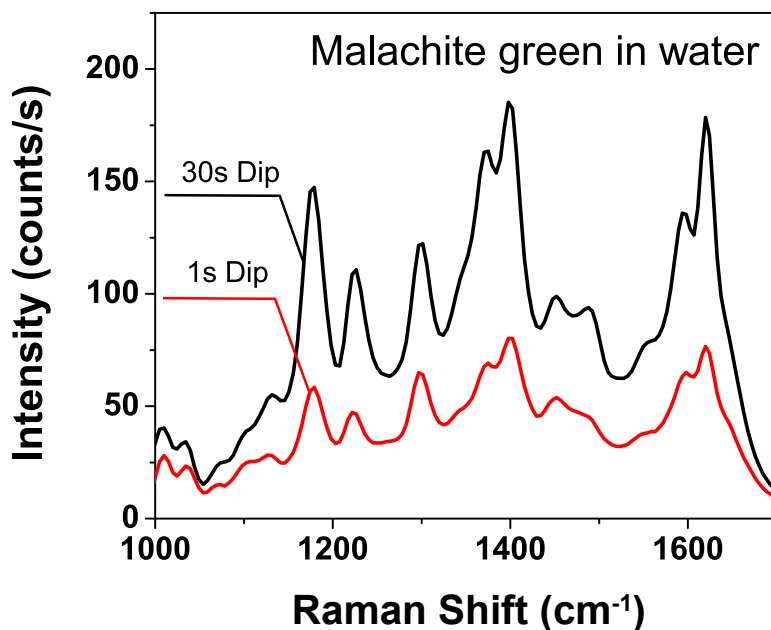
Figure 3.8: Comparison of signal intensity for 1 and 30 second dipsticks (1ppb malachite green in water).

3.3.5 Application: detection of fungicide residue on a surface

Potentially the most significant advantage of paper SERS devices as compared to rigid SERS substrates may be the capability to detect residues on surfaces. One can intuit that a silicon or glass SERS device cannot be used reliably to collect trace quantities of molecular residues directly from a surface, e.g., pesticide residue on a

produce item. In contrast, flexible SERS substrates can be used to wipe surfaces of complex topologies. In addition, the paper can be wet such that surface-bound residues can be drawn into the paper.

To illustrate the use of paper SERS devices in this application, the fungicide thiram was deposited in known quantities onto a glass surface and allowed to dry. Then, a paper-based SERS substrate that had been wet with acetone was used to swab the surface. The Raman spectra collected for 10 ng, 100 ng, and 300 ng of thiram deposited onto the surface are shown in Figure 9. Even with only 10 ng of fungicide present on the surface, the thiram Raman peak at 1384 cm^{-1} is easily detectable. Thus, it is evident that paper-based SERS devices can be used to easily detect trace chemical residues directly from surfaces. This capability is expected to lead to a range of new critical applications for SERS detection in the field.
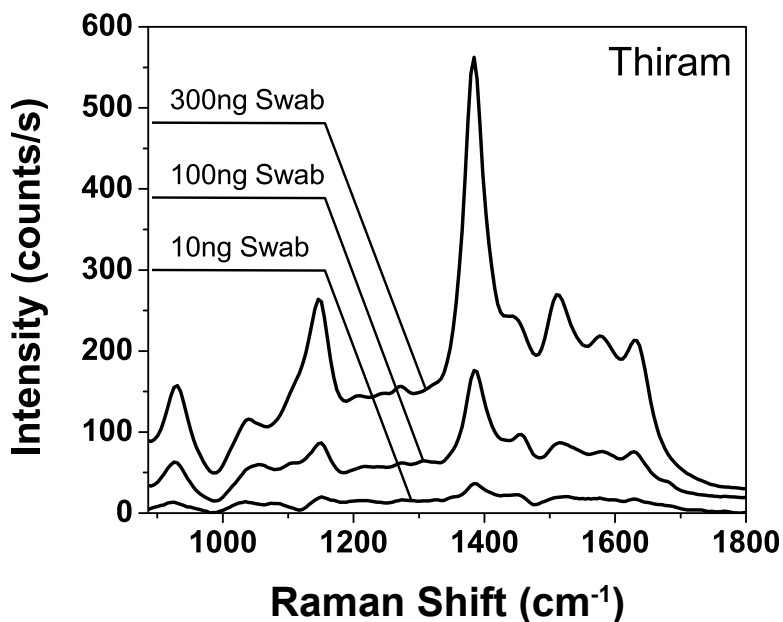
Figure 3.9: SERS signal obtained by swabbing glass slides with various amounts of thiram deposited on the respective surfaces.

44

3.4   Conclusion

We have developed a new method for the fabrication of SERS substrates by inkjet printing metal nanoparticles onto paper. These devices, which are highly sensitive and yet low in cost to produce, are optimized for rapid and portable chemical detection in the field. The sensitivity of the paper SERS devices is verified by detecting BPE in concentrations as low as 1.8 ppb. In addition to low cost and high sensitivity, the paper SERS devices feature unprecedented ease of use. Two real-world applications are demonstrated to illustrate the ease of use for chemical identification at the point of sample. First, the fungicide malachite green in water (1 ppb) is detected by simply dipping the paper SERS device into the sample, causing the analyte to be wicked into the sensor. Second, residue of the fungicide thiram is detected on a surface. A clear signal is observed even when only 10 ng of the fungicide is present on the surface. Importantly, these results are achieved with a low cost portable spectrometer, further emphasizing the application of the paper SERS devices for portable on-site detection. We believe that in the near future this new method of chemical identification has great potential to fill critical needs in food safety, environmental protection, and security.

In the next chapter, we present a novel assay which combines these paper-SERS sensors with PCR to enable highly multiplex detection of DNA targets within a single reaction.

Chapter 4

Multiplex detection of DNA targets using PCR and paper SERS

chromatography

4.1 Introduction

Rapid identification of infectious diseases is critical for improving patient quality of care, reducing healthcare costs and speeding recovery. Cultures are commonly used, however they are slow and provide limited information. Molecular diagnostics enable accurate and rapid detection [7], providing results in hours instead of days. Detection is commonly performed using polymerase chain reaction (PCR), which relies on the primer-directed exponential amplification of target DNA sequences [92].

It is well recognized that for an accurate diagnosis, the detection of multiple genes is required, especially in the case of suspected drug resistance. In a sophisticated and centralized clinical setting, this can be accomplished by running multiple PCR reactions, each aiming to identify a respective gene to form a complete diagnosis. However, to move toward a point of care model, it may be necessary to identify the presence of multiple genes in a single reaction due to limited resources and limited sample volume.

In principle, multiple targets within a single reaction can be screened for using quantitative real-time polymerase chain reaction (qPCR) in combination with

hydrolysis probes, utilizing the 5′ to 3′ exonuclease activity of the *Taq* DNA polymerase [69]. Hydrolysis probes (i.e. TaqMan®probes) use identifying fluorophore labels to indicate the amplification of multiple targets within a single reaction. These hydrolysis probes rely on a 5′ fluorophore and a 3′ quencher; when the probe is hydrolyzed during primer extension (indicating the presence of the target), the fluorophore is released and ceases to be quenched. While this technique is widely used, fluorescence has broad excitation and emission wavelengths and requires separate filters for each fluorophore, typically limiting assays to one or two targets per reaction.

In Chapter 3 we explored in depth paper-based substrates for surface enhanced Raman spectroscopy (SERS), an alternative transduction mechanism that leverages the highly specific and narrowband vibrational scattering features of Raman spectroscopy along with the optical enhancement provided by localized plasmonic resonances of metal nanostructures. Using a single excitation source and detector, SERS provides easily identifiable spectral bands which are unique to each molecule and serve as a molecular fingerprint for a target.

Here, we report an assay in which we combine the ink-jet printed paper SERS substrates from Chapter 3 with PCR to enable highly multiplexed detection of DNA targets. In addition, the chromatographic properties of paper are used to simplify the discrimination of Raman labels. These paper SERS devices offer a low-cost yet highly sensitive alternative to nano and micro-fabricated substrates, with the additional benefit of enabling chromatographic separation *within* the substrate itself.

In this work, paper SERS devices are combined with PCR and single-labeled

hydrolysis probes to perform multiplex DNA detection. As hydrolysis probe assays are a mainstream tool and have been well characterized [3, 66], the large body of existing work can be leveraged to improve the ease of adapting this assay to new targets. In this assay, the probes have a 5′ Raman reporter and bind to a complementary target DNA sequence which is bracketed by primers (Figure 4.1A). During extension of the target sequence, the *Taq* DNA polymerase will encounter this probe, and due to the 5′ to 3′ exonuclease activity of the *Taq* poymerase it will degrade the probe, releasing the Raman reporter.

A Hydrolysis PCR   **B** Sample Application   **C** Separation   **D** Detection

Polymerase: Primer: Probe:

·If target sequence is present, the primers and Raman-labeled probes bind
·*Taq* polymerase hydrolyzes bound probes during extension, releasing Raman reporters

·Following PCR, sample applied to lateral flow paper separation device
·The opposite tip is plasmonically functionalized by inkjet printing

·Released Raman reporters are carried to the detection region by the mobile phase; intact probes are not

·Raman reporters are detected by measuring the SERS signal with 532 nm excitation

Figure 4.1: Depiction of the SERS-PCR assay for DNA detection using Raman probes. (A) PCR is performed using single-labeled probes. If the target is present, the probe will be hydrolyzed during extension, releasing the Raman reporters. (B) The PCR reaction is applied to a dipstick with a printed SERS-active region at the top. (C) A separation is performed which allows the Raman reporters to migrate to the top, while retaining the whole probes at the bottom. (D) A 532 nm laser and Raman spectrometer are used to read the SERS signal from the top of the dipstick.

Following PCR, paper SERS devices double as separation matrices to enable discrimination between whole and hydrolyzed probes (where hydrolyzed probes indicate the presence of the target sequence in the sample). First, the PCR sample is

applied to one end of a paper chromatograph, opposite from the end which has been printed with a SERS-active region (Figure 4.1B). After allowing the device to dry, it is dipped into a sample vial containing the mobile phase (60% ethanol) in which the released Raman reporter is soluble, but the intact nucleic acid probe is not (Figure 4.1C). A simultaneous separation (within the sample vial) and concentration (above the lid) then occurs, driven by the evaporation of the mobile phase from the top of the dipstick. Thus, if the target sequence is present, the Raman reporter is released during PCR amplification and subsequently carried up the dipstick where it can be detected within the plasmonically-functionalized region at the top using SERS (Figure 4.1D). If the target sequence is not present, the nucleic acid probe remains intact and the attached Raman reporter cannot move up the dipstick: no Raman reporter will be detected when performing a SERS measurement. Importantly, due to the narrow-band nature of Raman, multiple targets can be detected simultaneously, offering a solution for multiplex DNA detection using a single excitation source and detector.

To illustrate the PCR-SERS-dipstick assay's multiplexing potential, we simultaneously detect two genes that convey drug resistance in Methicillin-resistant *Staphylococcus aureus* (MRSA). MRSA is one of the top causes of difficult to treat healthcare associated infections (HAIs) [93], resulting in close to 100,000 invasive infections per year in the United States [94]. By detecting the presence of two genes, *mecA* and *femB*, MRSA can be distinguished from other staphylococci with a high degree of certainty [95,96], enabling appropriate treatment and improved prognosis. While we chose MRSA as the illustrative application, there are scores of diagnostic

tests which benefit from simultaneously screening for multiple targets. As the core principles of this technique are consistent with conventional PCR assays, this assay could be rapidly adapted to enable screening for any targets of interest using a single reaction and a simple paper-based SERS detection.

4.2   Experimental

4.2.1   MRSA primer selection and optimization

Three sets of primers were obtained from Integrated DNA Technologies (IDT, Coralville, IA) for each of the two MRSA genes: one published and two custom primers (sequences in Table 4.1). Customer primers were selected using PrimerQuest from IDT and the published sequence for MRSA strain TCH70 [97], and were designed to all bracket the SERS probes (described later). Melting temperatures for candidates proposed by PrimerQuest were calculated using MELTING [98] with the Allawi 1997 nearest neighbor parameters [99] and the Owcarzy 2004 salt corrections [100] to ensure selected primers had similar melting temperatures (and which were about 5° C lower than the probes). All sequences were checked to ensure they were not prone to hairpin and dimer formation using OligoAnalyzer from IDT.

To select optimum PCR annealing temperatures gradient PCR reactions were conducted using a Bio-Rad MJ Mini Thermal Cycler. Gel electrophoresis was conducted with 1% agarose gels and typical running conditions (5 V/cm for 45 minutes). Gels were cast with SYBR Green I stain at approximately $0.3 \times$ concentration within the gel, and were imaged using a UVP Biospectrum Chemi HR 410 imaging system.

4.2.2 Polymerase chain reaction procedures

Custom DNA primers and probes (sequences in Table 4.2) were obtained from Integrated DNA Technologies (IDT, Coralville, IA). *Taq* DNA polymerase with ThermoPol® buffer, pUC19, dNTPs and the restriction enzyme *Ssp*I were obtained from New England Biolabs (NEB, Ipswich, MA). The pUC19 was linearized with *Ssp*I according to the NEB protocol (with a 5 times excess of enzyme). Genomic DNA from MRSA strain TCH70 was obtained from BEI Resources (Manassas, VA). For pUC19 experiments, thermocycling was conducted using a 10 second melt step at 95°C, a 15 second annealing step at 68°C and a 30 second extension step at 72°C. Cycling was repeated a total of 30 times and was followed by a final extension for 5 minutes at 72°C. For MRSA experiments, thermocycling was conducted using a 30 second melt step at 95°C, a 15 second annealing step at 61.6°C and a 15 second extension step at 68°C. Cycling was repeated a total of 30 times. PCR amplification was carried out in $1\times$ ThermoPol® buffer (20 mM Tris-HCl @ pH 8.8, 10 mM $(NH_4)_2SO_4$, 10 mM KCl, 2 mM $MgSO_4$, 0.1% Triton® X-100) with 200 μM dNTPs and 200 nM of primers and probes added. For the pUC19 reactions, 10^{10} copies of template DNA were used, while for the MRSA reactions 10^4 copies were used. In all cases, correct PCR product was verified by melt curve analysis and gel electrophoresis.

As the TCH70 strain of MRSA contains both the *mecA* and *femB* genes, a slight modification to these procedures was made to allow for simulation of single gene detection within a multiplex assay. In all experiments both MRSA probes

Table 4.1: DNA sequences investigated for use as MRSA primers and probes

Name	Oligonucleotide Sequence ($5' \rightarrow 3'$)	Product
mecA Fwd. Pub [101]	GTA GAA ATG ACT GAA CGT CCG ATA A	
mecA Rev. Pub [101]	CCA ATT CCA CAT TGT TTC GGT CTA A	479 bp
mecA Fwd. 1	CAA ACT ACG GTA ACA TTG ATC GC	
mecA Rev. 1	GCT TTG GTC TTT CTG CAT TCC	116 bp
mecA Fwd. 2	TTG ATC GCA ACG TTC AAT TT	
mecA Rev. 2	TCC TGG AAT AAT GAC GCT ATG	83 bp
femB Fwd. Pub [102]	TTA CAG AGT TAA CTG TTA CC	
femB Rev. Pub [102]	ATA CAA ATC CAG CAC GCT CT	651 bp
femB Fwd. 1	TAC GCC CAT CCA TCG TAC TT	
femB Rev. 1	CCA TTT GAA GGT CGC GAG AAA	120 bp
femB Fwd. 2	GCT CGA TGT ATC ATA CTC AGT TGT	
femB Rev. 2	AGA TAT CGT GCC ATT TGA AGG T	109 bp

Table 4.2: DNA sequences used for use in SERS PCR assay

Name	Oligonucleotide Sequence ($5' \rightarrow 3'$)	Product	$5'$ label
pUC19 Fwd.	GGA TTA GCA GAG CGA GGT ATG TAG		
pUC19 Rev.	GGT TTG TTT GCC GGA TCA AGA G	158 bp	
pUC19 Probe	TGG TAT CTG CGC TCT GCT GAA GCC AGT		CR6G
mecA Fwd.	CAA ACT ACG GTA ACA TTG ATC GC		
mecA Rev.	GCT TTG GTC TTT CTG CAT TCC	116 bp	
mecA Probe	AGA AGA TGG TAT GTG GAA GTT AGA TTG GGA		CR6G
femB Fwd.	GCT CGA TGT ATC ATA CTC AGT TGT		
femB Rev.	AGA TAT CGT GCC ATT TGA AGG T	109 bp	
femB Probe	AGC CAT GAT GCT CGT AAC CAT GTG A		TAMRA

were added to the reaction, however for the single gene experiments the primers corresponding to one of the genes were omitted.

4.2.3 Fluorescence measurements

In order to validate and optimize this assay, a second pUC19 probe (same sequence) was obtained with a 5′ TEX 615 label. Overlapping fluorescence images were collected using an Olympus IX51 microscope and manually aligned. These images were then analyzed using Image-J (National Institutes of Health) by averaging the fluorescence laterally (across the width of the chromatography strips, left to right in Figure 4.2A) to produce plots of fluorescence intensity as a function of distance traveled vertically. Data is plotted in terms of the retardation factor R_F, which is defined here as the ratio of distance traveled by the sample to the distance traveled by the solvent (with the position of the maximum fluorescence of the applied sample defined as $R_F = 0$ and the maximum extent of the solvent as $R_F = 1$).

4.2.4 Paper selection for chromatographic separation

An initial survey of paper for chromatography was conducted, comparing the separation performance offered by Fisher chromatography paper, VWR 1 μm filter paper and Whatman grade 1 (13 μm), 2 (8 μm) and 41 (20-25 μm) papers. A 30 bp DNA probe from Integrated DNA Technologies (Coralville, IA) with a 5 ′ carboxy Rhodamine 6G (CR6G) label was used as the model analyte (5′ → 3′ AGC
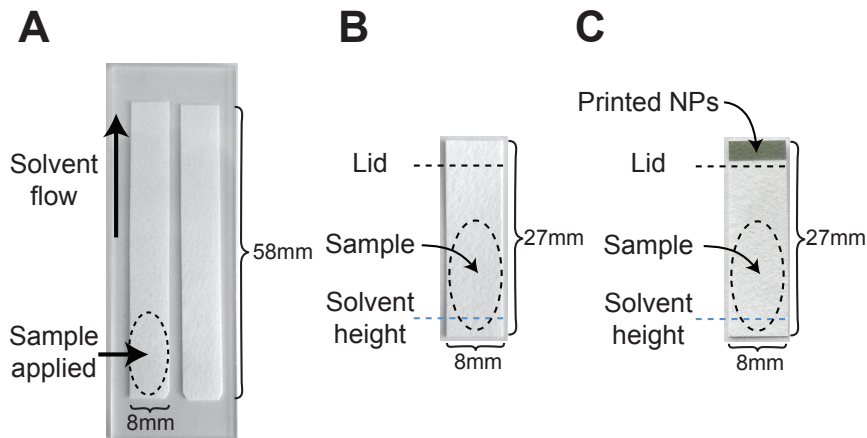
Figure 4.2: (A) Chromatography strips used for fluorescence validation of the assay. (B) Dipstick used for fluorescence validation of dipstick separation and concentration. (C) Dipstick with ink-jet printed SERS-active region for SERS experiments.

GTG GCG CTT TCT CAA TGC TCA CGC TGT). A portion of this probe was hydrolyzed at 10 μM concentration with DNase I (NEB, Ipswich, MA) according to the NEB recommended protocol (one unit per μg of DNA, except reacting for 60 minutes instead of 10 minutes).

First, 1 μL of 10 μM DNA (either hydrolyzed using DNase or whole) was pipetted a few mm from the bottom of the strips of paper. After allowing it to dry, the strips were dipped into vials containing either 50% or 70% ethanol and allowed to run for 15 minutes. After being removed and dried, the strips were imaged using a 302 nm transilluminator and SYBR®Gold filter on a UVP Biospectrum Chemi HR 410 imaging system.

To compute the integrated intensity, a background subtraction was conducted by subtracting the average intensity from an unused piece of paper from the chromatographs. Following the background subtraction, a simple numerical integration was performed from $R_F = 0.3$ to $R_F = 1.0$.

4.2.5   Chromatographic separation

To evaluate the chromatographic separation of the PCR samples, entire PCR reactions (20 μL) were applied to the bottom of 8×58 mm chromatography strips made from Whatman Grade 2 paper (as shown in Figure 4.2A), and allowed to dry. The entire strip was suspended in a sealed jar such that the bottom 3 mm of the strip was immersed in the mobile phase. The chromatography strip was allowed to run for 15 minutes (solvent reaching approximately 43 mm) before being removed and dried for fluorescence evaluation.

To compute the integrated intensity, first a background subtraction was conducted for each sample by subtracting the average intensity of the upper end of the chromatography strip (above $R_F = 1$). Then a simple numerical integration was performed from $R_F = 0.3$ to $R_F = 1.0$.

4.2.6   Silver nanoparticle ink synthesis

The silver colloid was synthesized using the simple reduction reaction method of Lee and Meisel [55]. Silver nitrate, sodium citrate and dextran (average MW 150,000) were obtained from Sigma-Aldrich (St. Louis, MO). Briefly, 72 mg of silver nitrate was added to 400 mL of DI water (18.2 MΩ) and brought to a rapid boil in a 500 mL Erlenmeyer flask. While stirring quickly (such that the vortex reaches the bottom of the flask), 80 mg of sodium citrate in 1 mL of water was added. The color slowly changed to a green-brown color. After 10 minutes the solution was removed and allowed to cool to room temperature.

The silver ink was formed by first concentrating the silver colloid $100\times$ through centrifugation at $3{,}000g$. Then 5 mg/mL dextran in water was added to the concentrated colloid at a 1:1 ratio.

4.2.7 SERS substrate printing

Printing was performed as previously described [56, 86]. After injecting the ink into refillable ink cartridges from Alpha D Development Inc. (Lakeland, FL), a consumer piezo-based ink-jet printer (Epson Workforce 30) was used to print onto untreated filter paper (Whatman Grade 2). To increase the nanoparticle concentration in the substrate, the printing was repeated five times.

4.2.8 Dipstick separation and concentration

For fluorescence validation of the SERS devices, 8×27 mm dipsticks were used (Figure 4.2B). The bottom 3 mm of the dipstick was dipped in 60% ethanol in a vapor saturated vial while the top 3 mm of the dipstick was allowed to emerge from the vial through a slit in the lid. This not only promotes a chromatographic separation within the sample vial, but allows for an evaporation-driven concentration of Raman reporters near the top of the paper strip, where the sensing region would be located. Similar dipsticks, this time with printed silver regions at the top, were used for the SERS experiments (Figure 4.2C).
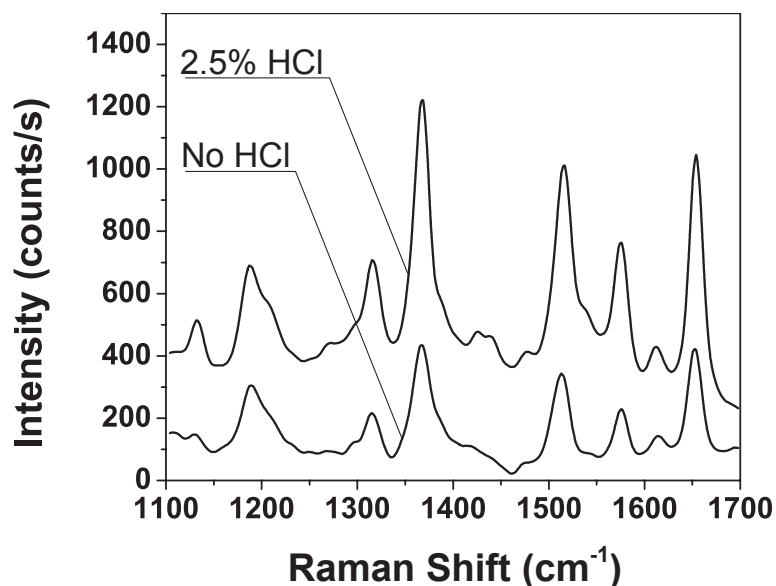
Figure 4.3: Representative spectra showing the effect of adding acid to the dipstick SERS-active region before measurement.

4.2.9 SERS measurements and analysis

SERS measurements were performed using a 532 nm laser (0.6 mW) for excitation. This wavelength overlaps with the optical absorption of the Raman labels used in this report, enabling a resonance SERS enhancement. A Horiba Jobin Yvon LabRam ARAMIS Raman microscope was used for detection. Measurements were rastered over a 200×200 μm region by the system twice per integration period. An integration time of one second with 5 averages was used for all measurements. Immediately before measuring, 2 μL of 2.5% HCl was applied by pipette to the center of the printed region to protonate the Raman reporter and promote interaction with the nanoparticles (representative spectra shown in Figure 4.3). Using an automated stage, measurements were taken in two rows of 3 equally spaced locations. The combination of rastering, averaging and imaging multiple locations substantially reduces the signal variability due to the uneven nature of chromatographic separation and

concentration; for each of the 5 positive pUC19 dipsticks shown here, the relative standard deviation, $|\sigma/\mu|$, of the 1510 cm^{-1} peak height (one of the common peaks used for identification) ranges from 15 to 29%. For quantification of the singleplex data (using pUC19 as a model target), the magnitude (in photon counts per second) of the 1510 cm^{-1} peak was computed by taking the difference between the magnitude of the peak and the nearest local minimum. For display, each dipstick's 6 spectra were averaged together and a linear fit was subtracted (to reduce the contribution of fluorescence). A 5 point FFT smoothing filter was applied before plotting.

4.3 Results and discussion

4.3.1 Experimental selection of chromatography paper

As this assay relies on the chromatographic discrimination capability of the paper dipsticks to differentiate between whole probes (no target) and hydrolyzed probes (target present in PCR reaction), the appropriate selection of a paper is an essential consideration. There are two aspects of paper selection to consider. First, the paper has to provide a good signal contrast between whole and hydrolyzed DNA probes. Second, the paper has to be able to serve as a good matrix for an ink-jet printed SERS substrates.

The first step in the selection process was to investigate the chromatographic separation performance of various paper options available to us. To compare the paper options, DNA samples (whole or hydrolyzed with DNase) were pipetted onto paper strips a few mm from the bottom. After performing a 15 minute chromato-

graphic separation, the strips were imaged and a background subtracted integrated

intensity was computed, running from just past the top of the applied sample lo-

cation to the top of the paper. Results are displayed in Figure 4.4. The goal is to

have the most contrast possible between the whole and hydrolyzed DNA probes.

As can readily be seen, Whatman grade 1 and 2 papers (70% ethanol in water as

running solution) as well as VWR 1 μm paper (50% ethanol in water) offered the

best contrast (indicated by red boxes).
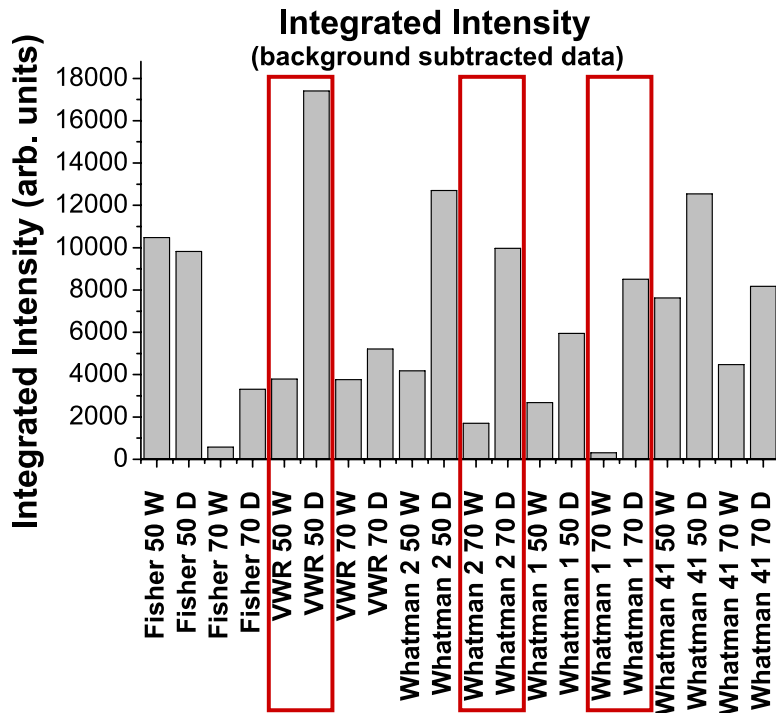
Figure 4.4: Integrated intensity of background subtracted data,
demonstrating maximum contrast with VWR 1 μM and Whatman
grade 1 and grade 2 papers. W = whole DNA probe, D = hydrolyzed
(using DNase) DNA probe. Data shown for both 50% and 70% ethanol
in water.

Having identified the best paper selections for separating whole from hy-

drolyzed DNA, we then evaluated the SERS performance on each of these papers.

The integrated intensity of the 1513 cm^{-1} peak is plotted in Figure 4.5. The VWR 1 μm paper displayed the poorest SERS performance. Due to the small pore size, an over-aggregation of the metal nanoparticles was observed, giving a reduced SERS signal as well as a high background signal from the silver nanoparticles. Both of the Whatman papers gave reasonable SERS results, and Whatman grade 2 paper was selected for further experiments due to its smaller pore size which is expected to give better separation results based on the results seen in Figure 4.4.
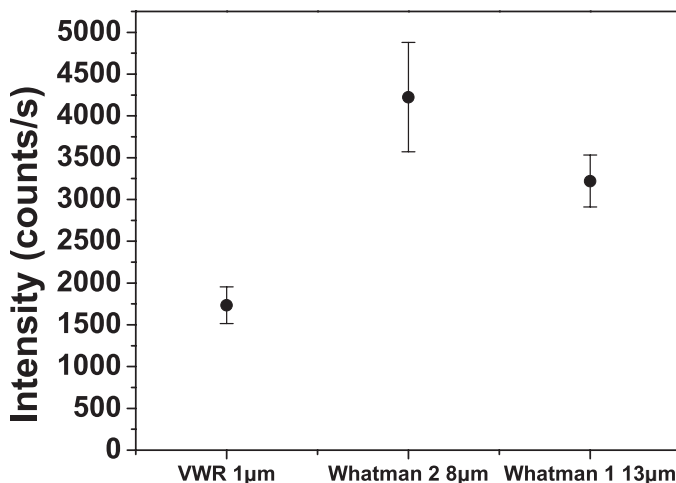
Figure 4.5: Comparison of SERS performance of ink-jet printed AgNPs on papers demonstrating maximum chromatographic contrast between whole and hydrolyzed DNA. Varying numbers of print cycles were tested for each paper, and the number of cycles giving the largest signal for 2 μL 10μM Rhodamine 6G (R6G) is displayed here as the magnitude of the 1513 cm^{-1} peak. n = 3 for each sample.

4.3.2 MRSA PCR primer selection and duplex PCR verification

In order for the duplex assay to be successful, the primers used for amplification must have similar melting temperatures and thus amplification efficiencies. If the

primers are not well matched, one primer can dominate the reaction, and due to the exponential nature of PCR amplification it will deplete the reagents and the other target will not be detected. Three sets of primers were evaluated for each gene target: one published and two custom primers. A gradient PCR was conducted in which each primer set was subjected to four different annealing temperatures (otherwise the PCR reaction was run as usual). PCR products resulting from this gradient PCR were visualized using agarose gel electrophoresis, as seen in Figure 4.6.
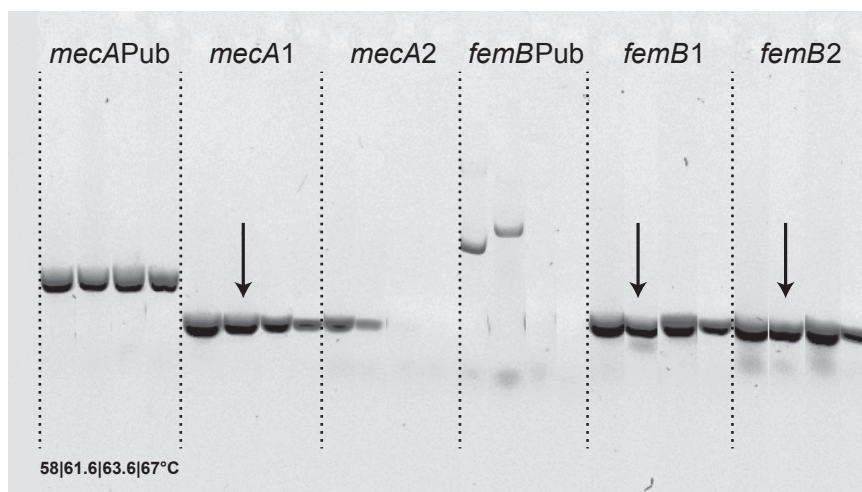
Figure 4.6: Gel electrophoresis images showing results for PCR amplification using primer sets for the MRSA genes *mecA* and *femB*. Gradient PCR conducted with annealing temperatures at 58, 61.6, 63.6 and 67°C. PCR protocol otherwise matches that reported in Section 4.2.2.

Of the primer sets evaluated, two were immediately disqualified based on the gradient PCR result: the second custom *mecA* primer set as well as the published *femB* primer set. As the product length of the published *mecA* primer set is quite long, we narrowed our selection to the first custom *mecA* primer set and both custom

61

femB custom primer sets. PCR reactions were then conducted investigating duplex PCR reactions with these primers which resulted in the first custom *femB* primer set being eliminated due to dimer formation with the *mecA* set.

Having selected the *mecA*1 and *femB*2 primer sets as the optimal primer sets to be used in subsequent experiments, we then attempted to validate the duplex PCR reaction. Real-time PCR was used since the products produced by these primers are about the same length, making a size based separation like gel electrophoresis ineffectual. In order to confirm that duplex PCR was happening as expected, PCR reactions were conducted with either the *mecA*1, *femB*2 or both primer sets (duplex). Then, these reactions were used as the template for $1/20^{\text{th}}$ of a second PCR reaction. The real-time PCR results from this second reaction are displayed in Figure 4.7.
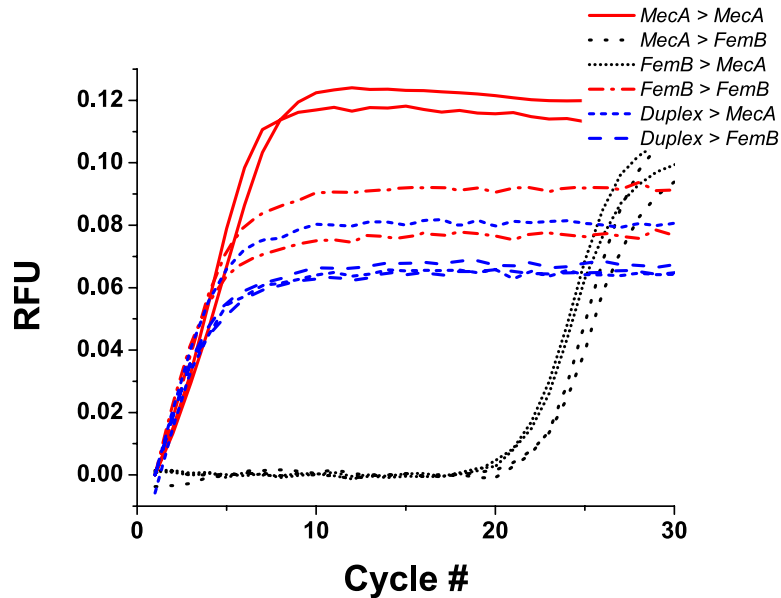
Figure 4.7: Real-time PCR verification of duplex PCR using *mecA*1 and *femB*2 primer sets (1× SYBR Green I added to PCR reactions to allow visualization of amplification)

As can be seen, when the second PCR reaction is conducted with the same primers as the original reaction, amplification occurs almost instantly. The same happens when the duplex reactions are used as template for PCR reactions with either of the gene primer sets. However, when a PCR reaction for one gene is matched with primers from the other gene, amplification happens very slowly, consistent with a $1/20^{th}$ dilution of the MRSA template in the first PCR reaction.

Further verification of the PCR reaction can be obtained by performing an amplification with either *mecA*1, *femB*2 or both primer sets, and subsequently performing a melting curve analysis. Figure 4.8 confirms the appropriate duplex amplification in two ways. First, the duplex PCR reaction amplifies about one full cycle faster than the singleplex reactions, which is consistent with a reaction which is beginning with twice as many segments of DNA which can be amplified. Second, the melting curve analysis in Figure 4.8 shows unique melting temperatures for each primer set, and a combination of both for the duplex reaction.

4.3.3 Experimental selection of the chromatography mobile phase

The PCR probes employed for this assay have a $5'$ Raman reporter and a $3'$ phosphate to prevent extension of the probe. As the primers are extended the *Taq* polymerase will encounter and hydrolyze the probe (Figure 4.1). This results in the Raman reporter being released from the probe along with a few residual bases [69]. As a result of this less than perfect hydrolysis, the parameters of the separation are critical. The percentage of ethanol (in water) used as the mobile
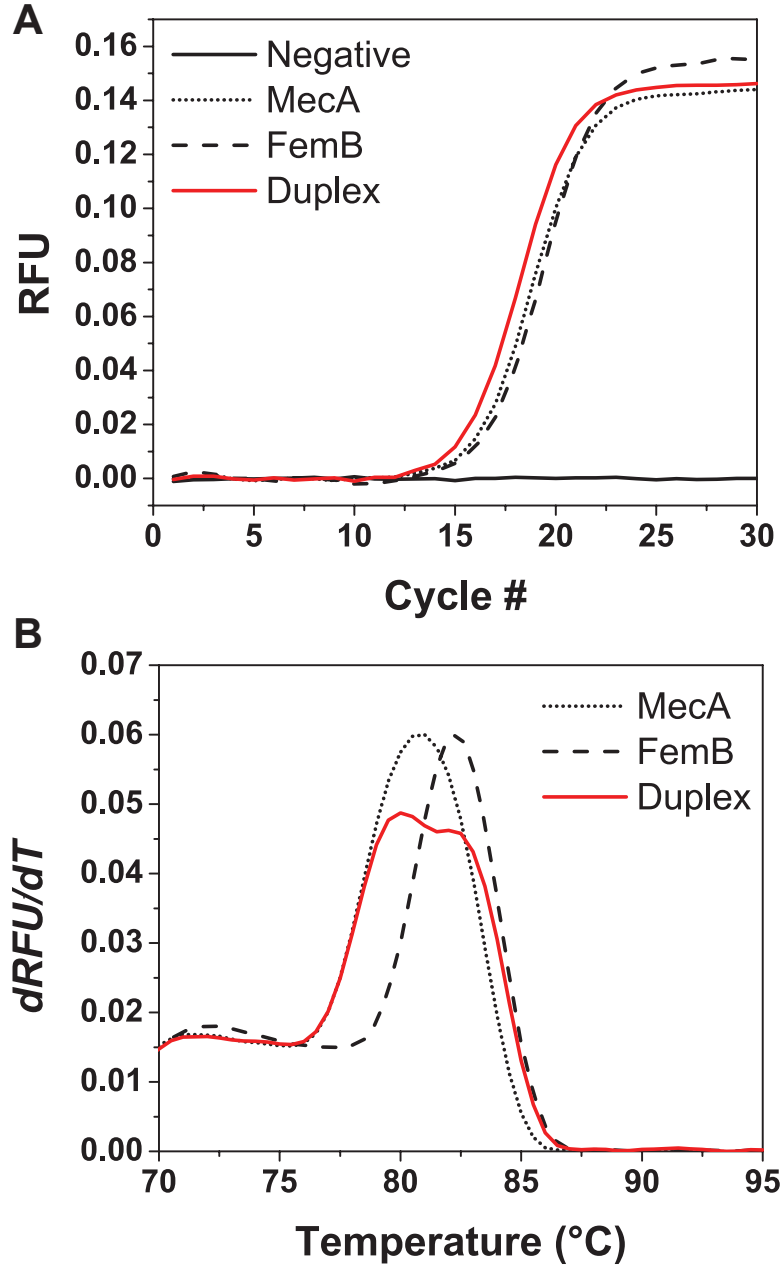
Figure 4.8: (A) Representative real-time PCR amplification results using *mecA*1 and *femB*2 primer sets (1× SYBR Green I added to PCR reactions to allow visualization of amplification). Duplex amplification becomes visible about 1 cycle sooner than the single gene amplifications, implying that the duplex PCR is amplifying two targets. (B) Representative melt curves for PCR amplification using *mecA*1 and *femB*2 primer sets. Double peak in duplex results indicates desired amplification of both targets simultaneously.

phase was adjusted for optimal signal contrast between the negative and positive PCR samples. Chromatography was performed comparing positive (pUC19 present in reaction) and negative (no pUC19) PCR samples. To investigate the chromatographic separation, fluorescence microscopy and bare (no nanoparticles) paper was employed. Chromatographs for three different concentrations of ethanol were collected and analyzed by conducting a background-subtracted integration as shown in Figure 4.9 (raw chromatographs in Figure 4.10). As can be seen, both released Raman reporters and intact probes were mobile in 50% ethanol. Both 60% and 70% ethanol significantly reduce the signal for the negative samples, and it can be seen that 60% ethanol offers the best contrast between the positive and negative samples.
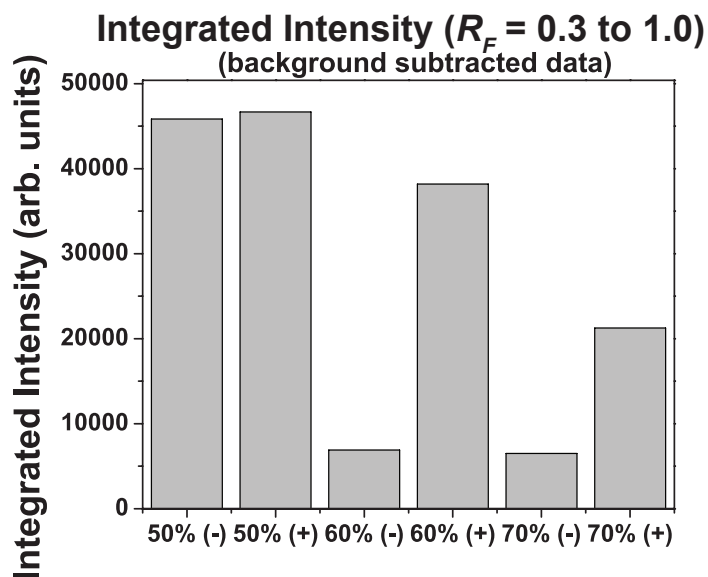
Figure 4.9: Integrated intensity of background subtracted data, demonstrating maximum contrast with 60% ethanol.

To further improve signal contrast between the positive and negative samples, a simultaneous separation (below the vial lid) and concentration (above) is used, in
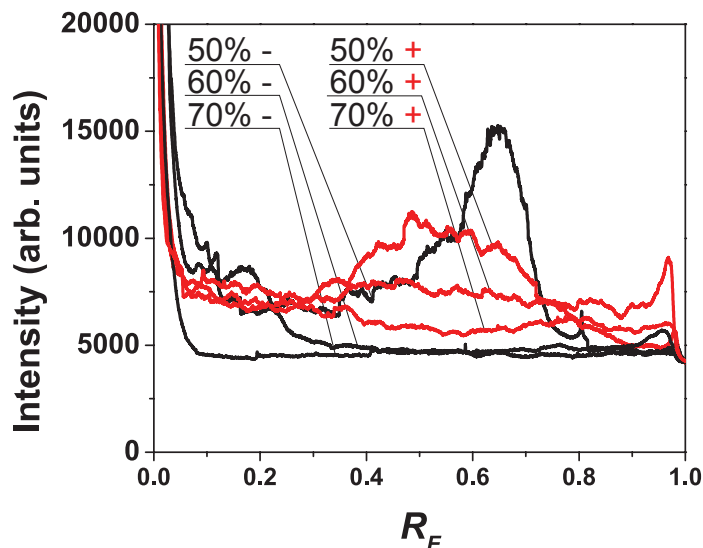
Figure 4.10: Fluorescence intensity (averaged across the width of the
strips) demonstarting the chromatographic differentiation between
positive (red lines, target in reaction) and negative (black lines, no
target) as a function of ethanol concentration in the mobile phase.

which a continual evaporation-driven deposition of Raman reporters occurs above

the lid. The resulting chromatographs for three different dipstick running times

are shown in Figure 4.11. An essentially zero fluorescence is observed for the nega-

tive samples, while increasing fluorescence is observed with increasing time for the

positive samples, demonstrating the effectiveness of the combined separation and

concentration.

4.3.4   SERS detection of the PCR reaction

Having established the ability of a chromatography dipstick to both discrim-

inate and concentrate reporters, we then investigated the use of SERS to detect

Raman reporters from PCR samples. As in the chromatography experiments, the

full 20 μL post-PCR sample is applied to the bottom of the dipstick and allowed to
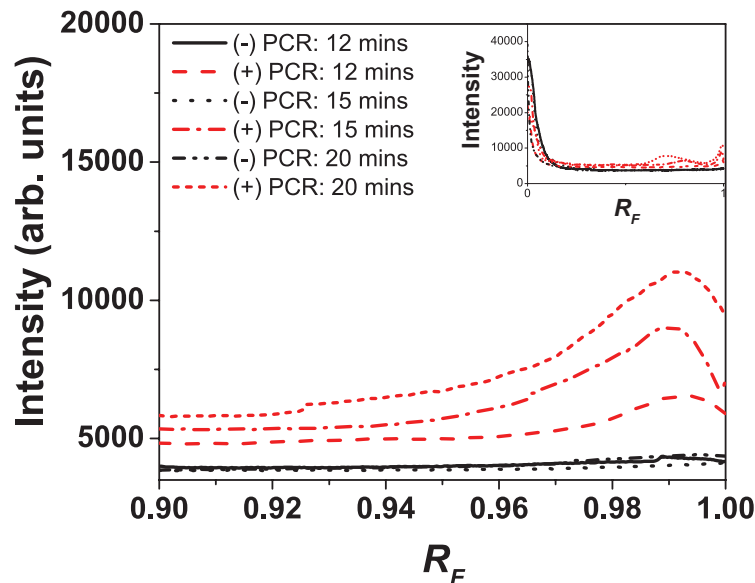
Figure 4.11: Fluorescence intensity (averaged across the width of the strips) showing the fluorescence intensity vs distance for a number of different running times (60% ethanol mobile phase)

dry. After running the dipstick for 20 minutes, acid is added to protonate the Raman reporter and the SERS signal is immediately measured. Representative traces for 10 dipsticks using pUC19 as a model target (5 positives and 5 negatives) are shown in Figure 4.12A. Three prominent peaks of CR6G which are commonly used for identification and quantification are indicated with asterisks (1310, 1360 and 1510 cm^{-1}). Averaging the spectra obtained at 6 different locations within the dipstick enables us to obtain relatively consistent signal magnitudes for both the positive and negative dipsticks, as shown in Figure 4.12B, allowing for clear and reliable differentiation between positive and negative results.
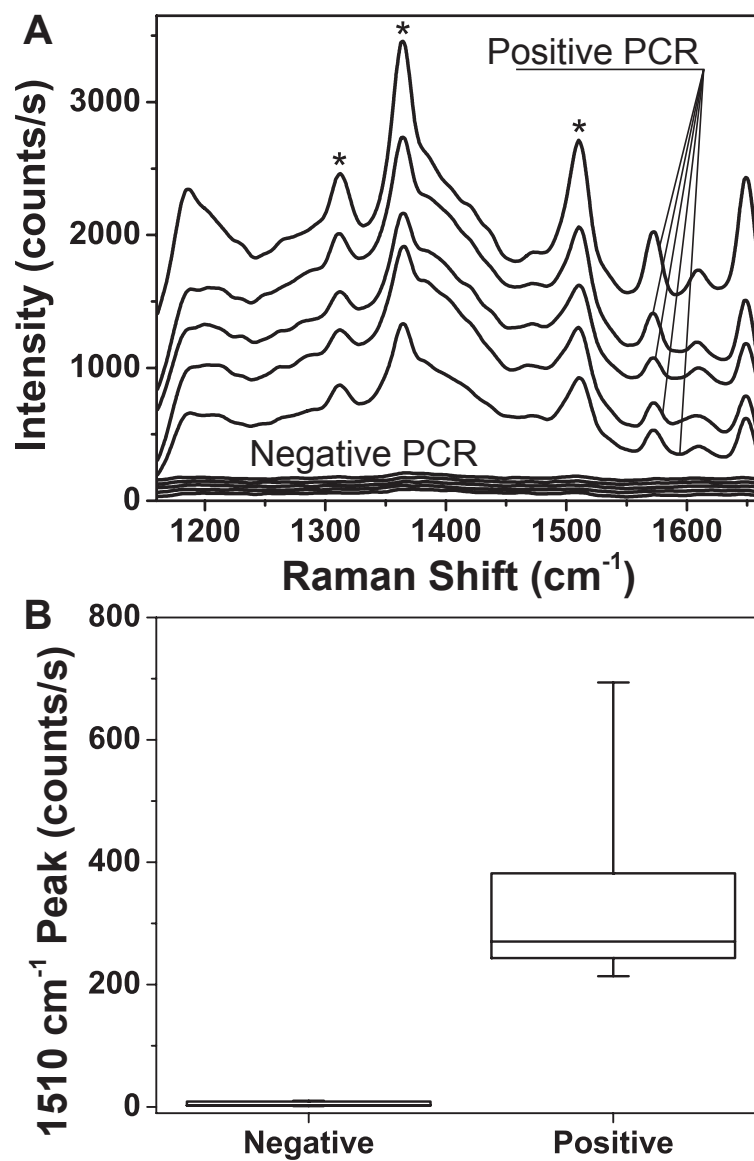
Figure 4.12: Simultaneous separation and concentration is performed using SERS dipsticks and PCR samples. (A) Representative SERS spectra from 5 positive (reaction containing target) and 5 negative (no target) dipsticks are shown (shifted vertically for clarity). Reprinted from Hoppmann, et al., in press [5]. (B) Box plot of 1510 cm^{-1} peak height for these 10 spectra.

4.3.5 Multiplex detection of MRSA genes

To demonstrate the feasibility of this technique as a multiplex diagnostic tool, we then applied this technique to the detection of the MRSA genes *mecA* and *femB*, two genes responsible for MRSA's antibiotic resistance. Four different scenarios were investigated: samples containing 10^4 copies of MRSA (about 30 pg), samples containing only *mecA* or *femB* (simulated by omitting a primer set), and samples with no target DNA at all. Three PCR reactions followed by SERS dipsticks were performed for each of these cases, for a total of 12 experiments. Representative traces of each of these possibilities are shown in Figure 4.13A. The characteristic peaks that were used for identification of the *mecA* Raman reporter CR6G and the *femB* Raman reporter tetramethylrhodamine (TAMRA) are indicated with asterisks and triangles, respectively. These spectra can be compared to reference spectra of the two dyes deposited directly on printed silver (Figure 4.14). The ability to consistently obtain results enabling clear identification of all targets present in a sample is suggested by the three duplex results in Figure 4.13B. Control experiments were conducted in which the PCR reactions were directly pipetted onto the silver region of the dipsticks: for each case (negative, single gene, duplex) the spectra obtained matched the duplex result (Figure 4.15) indicating that the discrimination seen in Figure 4.13A is indeed due to the chromatographic properties of the paper substrate.
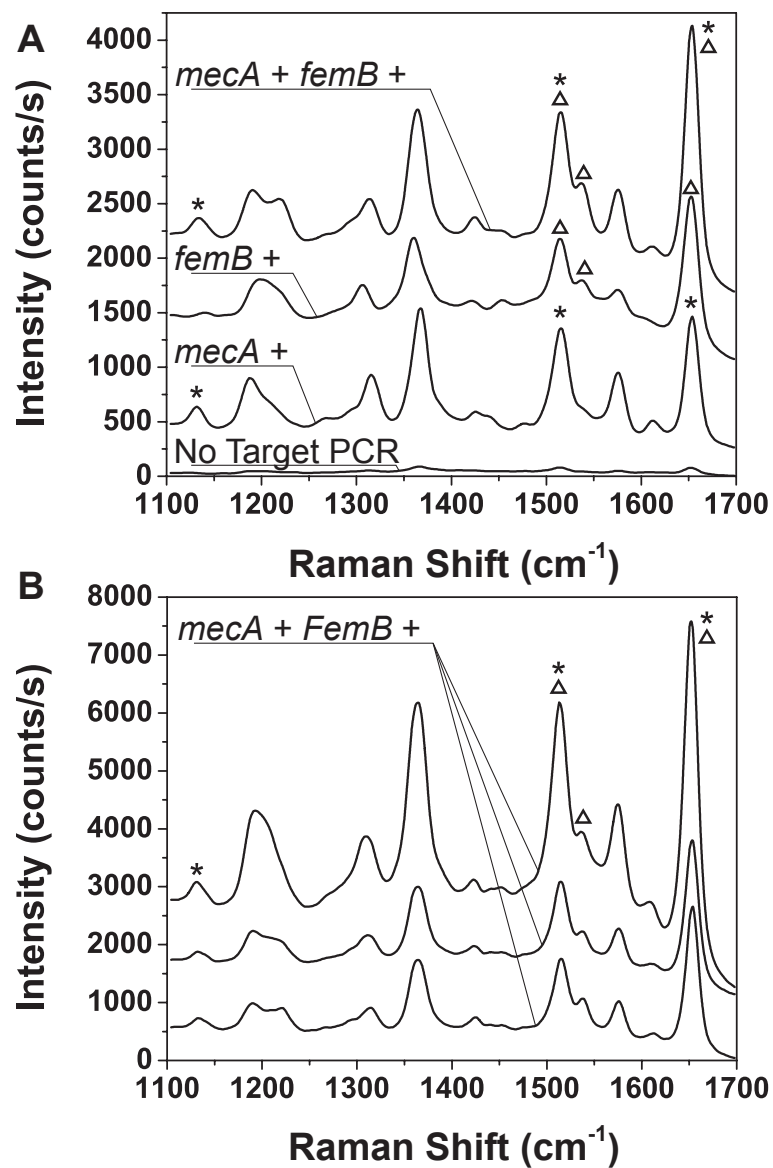
Figure 4.13: (A) Representative SERS spectra of results obtained from dipsticks with PCR reactions containing no target (but all probes and primers), only one gene (simlated by adding both probes but only one primer set) and both MRSA genes. (B) Three representative SERS spectra from duplex PCR dipsticks.
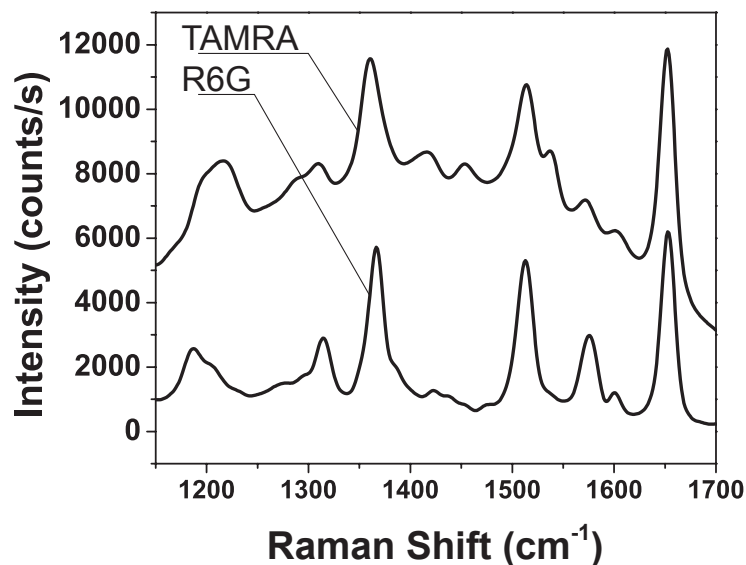
Figure 4.14: Reference SERS spectra of the two Raman reporters used on DNA probes. 2 μL of 10 μM pure dye in water was applied directly to the printed region and measured (0.06 mW laser power).
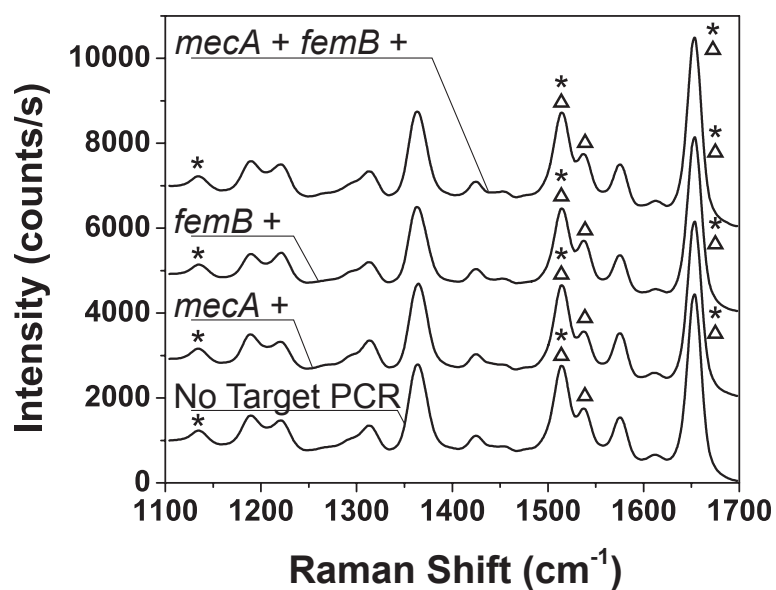
Figure 4.15: Control experiment showing SERS signals obtained by directly pipetting PCR reactions containing no target, one gene and both MRSA genes directly onto the printed SERS-active region (rather than running a dipstick).

4.4   Conclusion

A plethora of research results exist which demonstrate the power of SERS as a highly multiplexible detection modality, however the current methodologies for DNA detection require complex and expensive procedures. We have demonstrated the feasibility of a simple paper-based SERS assay to clearly and consistently discriminate between DNA targets in multiplex PCR reactions. By leveraging the unique chromatographic properties of the paper SERS substrates for discrimination, we eliminate the need for the user to perform complex sample processing steps that are usually required before SERS measurement. Fluorescence techniques have similar sensitivity to SERS, however the broad-band nature of fluorescence severely limits the number of simultaneous targets that can be detected in a fluorescence assay, and multiplex detection of even a few targets results in rapidly increasing equipment complexity. SERS offers highly multiplex detection using only a single excitation source and detector, making it well suited to point of care applications where it may be necessary to identify the presence of multiple genes in a single reaction due to limited resources and sample volume. We envision that, in combination with a low cost thermocycler and a commercially available handheld spectrometer, this approach could contribute to the development of DNA diagnostic tests enabling screening for a large number of targets within a single reaction.

Chapter 5

Statistical analysis for highly multiplexed SERS

5.1   Introduction

As has been seen in Chapter 3 (chemical detection) and Chapter 4 (DNA detection), surface enhanced Raman spectroscopy (SERS) presents an intriguing alternative to traditional detection modalities which is well suited for multiplex detection of analytes. However, in spite of this significant promise, only a few groups have attempted to experimentally demonstrate this potential [4,84,103], with most studies only using 2 or 3 targets at any one time. The reason for this is simple: as the number of SERS targets is increased beyond around 2 or 3, visually differentiating and analyzing the resulting spectra becomes impossible, even for a highly trained technician. Assays involving non-ideal targets (differing affinities for SERS substrates and unequal Raman cross-sections) further compound the difficulty. Nevertheless, in order for techniques such as the multiplex DNA assay presented in Chapter 4 to reach their potential, these difficulties must be overcome.

The need to analyze convoluted and highly dimensional signals is not unique to SERS: it is seen in numerous fields including chemistry and biology. Solutions to problems of these types are broadly classified under the field of chemometrics, a field which is focused on chemical data-analytics using multivariate statistics and other mathematical/computational techniques. Due to the typical nature of such data

(involving many interrelated variables and multiple components), extensions beyond univariate analysis (e.g. ordinary least-squares regression (OLS)) were sought. Two of the most frequently used multivariate analytic techniques are principal component regression (PCR) [104] and partial least-squares regression (PLS) [105, 106]. While alternate techniques such as ridge regression [107] and neural networks [108, 109] exist, they are not investigated here as they lack the ability of techniques such as PCR and PLS to reduce data dimensionality by selecting components which identify the most variation in the data [110], a very useful property when dealing with highly dimensional spectra. Differences are summarized in Table 5.1.

PCR[2] is a linear method which transforms the matrix of x-data to a new coordinate system defined by latent variables (components). These components are designed to be uncorrelated with one another (orthogonal), with each element accounting for the maximum variance in X possible [104]. OLS regression is then performed on the transformed data. While PCR usefully reduces dimensionality, by mathematical design it is only capable of identifying variability in X; while it is frequently used as a tool to discriminate between groups, it has no inherant capability for distinguishing groups [111].

PLS also transforms the data into a set of latent variables which are subsequently used for regression. The key difference between PLS and PCR is that while PCR seeks latent variables which maximize variability in X, PLS seeks components which maximize covariance between $\mathbf{X}$ and $\mathbf{Y}$, providing accurate models of the relationship between X and Y with fewer components than would be required with

---

[2]Not to be confused with polymerase chain reaction (PCR) from the preceding chapters.

Table 5.1: Comparison of selected regression techniques, adapted from [1].

Method	Highly Dimensional x	Collinear x Vars.	Components	y Involved in Model of x
OLS	N	N	N	Y
PCR	Y	Y	Y	N
PLS	Y	Y	Y	Y
Ridge	Y	Y	N	Y
ANN	Y	Y	N	Y/N

PCR [111].

Here we investigate the application of PLS to the analysis of 5 SERS analytes, ranging from $1\times$ to $5\times$ multiplexing. The application of asymmetric least-squares baseline subtraction to SERS data is presented. Selection of an optimal number of PLS components is discussed in the context of generating a good fit without overfitting the data. Accuracy of the PLS model when tested using leave-one-out cross-validation is presented. Sources of error and possible improvements are presented, with examples.

5.2 Experimental

5.2.1 SERS substrate preparation

SERS substrates were prepared similarly to those in Section 3.2.1, with a few minor differences. The paper used was Whatman grade 1 filter paper. The substrates were printed five times with the gold ink previously described, and were cut as shown in Figure 3.1B.

5.2.2   Sample preparation

5 test analytes were used for these multiplexing experiments: Rhodamine 6G (R6G), 1,2-Di(4-pyridyl)ethylene (BPE), Cresyl Violet acetate (CV), Methylene Blue (MB) and Malachite Green oxalate (MG). BPE, CV, MB and MG were obtained from Sigma Aldrich (St. Louis, MO) while R6G was purchased from Exciton (Dayton, OH). Stock solutions were prepared at 10 mM in Methanol, then diluted to 1 mM concentration in water. These 1 mM solutions were then used to generate 1 mL samples at 10 μM concentration in water for SERS analysis.

31 different samples were generated in this manner to allow investigation of all 31 possible combinations of analytes (five singleplex, ten duplex, ten 3-plex, five 4-plex and one 5-plex). For all of these samples, the concentration of each respective analyte was 10 μM.

5.2.3   SERS measurements

SERS measurements were collected using a 785 nm laser (17 mW) for excitation, a QE65000 (Ocean Optics) portable USB spectrometer for detection and a fiber optic probe (Agiltron) for delivery of laser light and collection of scattered photons. An integration time of one second was used for all measurements; signals represent the average of five measurements. Averaging was used to reduce the random background noise contributed by the detector. A linear translation stage was used to position the fiber optic probe.

For each sample, an ink-jet printed SERS substrate was placed on a glass slide

and 2 μL of sample was pipetted onto it. Spectra were collected from 5 different locations for each substrate.

5.2.4 Data pre-processing

Pre-processing of data is desirable to maximize the effectiveness of chemometric analysis. Care must be taken, however, as signal variability which contains valuable information can easily be removed by preprocessing reducing the effectiveness of the subsequent analysis. High-frequency noise (e.g. detector noise) which is unrelated to the actual measurement should be removed (unnecessary in our data). Low-frequency signal backgrounds should also be removed as these can reduce the effectiveness of the analysis. Differentiation is one option, however for our data it was found that this removed valuable information contained in the intermediate-frequency signal. Instead, a baseline technique which follows the general shape of the data, but allowing for intermediate-scale departure from the baseline was used: an asymmetric least-squares (ALS) baseline estimation [112, 113].

The ALS estimation is an iterative fitting process which is controlled by two parameters. The asymmetry parameter p defines the weight given to points above the fitted curve; small values of p ($p \ll 1$) cause the large peaks in the data to be mostly ignored by the fitting algorithm, which is ideal for SERS spectra. The λ parameter is a roughness penalty; smaller values of λ allow for tighter fitting to the data, while larger values give a smoother result. A representative example of an ALS fit of our data is shown in Figure 5.1. Values of $\lambda = 10^4$ and $p = .001$ were

interactively selected to give a fit that follows the valleys in the spectra without following too closely and removing valuable information (e.g. around 1400 cm^{-1} in Figure 5.1). These parameters were used to perform a baseline subtraction of the entire data set.
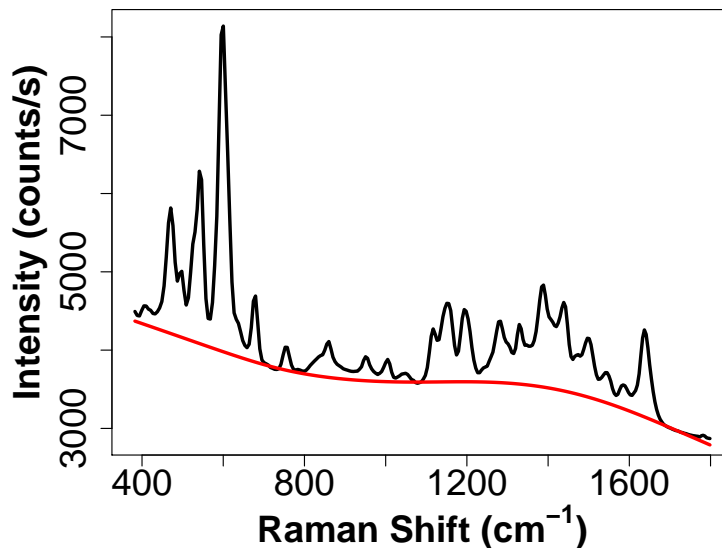
Figure 5.1: Baseline subtraction used to pre-process data before analysis. Raw data is in black, and the red line is the baseline to be subtracted. Asymmetric least-squares baseline fitting with the smoothing parameter $\lambda = 10^4$ and the asymmetry parameter $p = .001$ was used.

Representative background-subtracted spectra for the 5 singleplex samples as well as the 5-plex multiplex sample are shown in Figure 5.2. Further examples of places were over-fitting of the background could have been detrimental can be seen from 1300-1400 cm^{-1} in the bottom black multiplexed trace, as well as around 1400 cm^{-1} in the top gray trace.
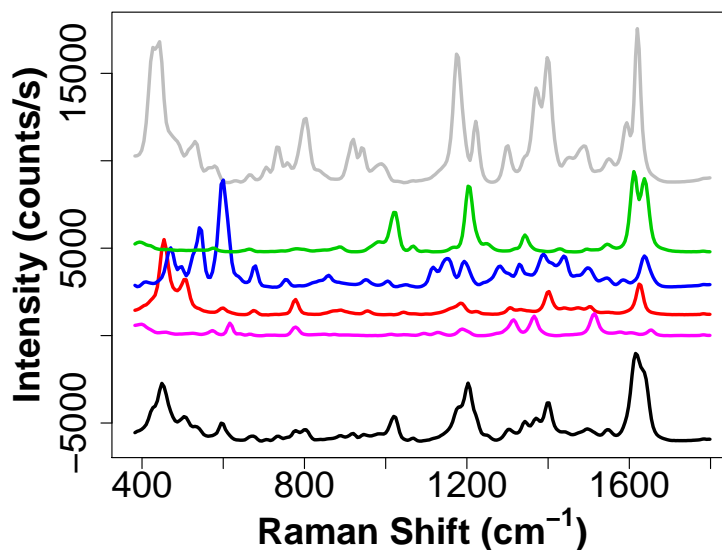
Figure 5.2: Representative spectra singleplex analytes, as well as a representative 5× multiplex result. From bottom to top: 5× multiplex result (black), R6G (magenta), Methylene Blue (red), Cresyl Violet (blue), BPE (green) and Malachite Green (gray). Shifted vertically for clarity.

5.2.5 PLS data analysis

PLS regression was applied to enable multiplex data analysis beyond the point where manual analysis can effectively differentiate the spectra of the analytes. This analysis was conducted using leave-one-out cross-validation (LOOCV), in which a single observation of the total data set ($n = 5 \times 31 = 155$) is removed (leaving 154 observations), PLS regression is conducted, and then the PLS model is used to predict the removed observation. This was repeated n times, offering a good estimation of actual model predictive performance in aggregate (this assumption is true as long as data points not replicated, e.g. two spectra collected back to back from the same location on the same substrate).

Following generation of PLS models using LOOCV, the number of components

to be used for further analysis is selected. To aid in this selection, plots of root mean square error of prediction (RMSEP) vs. number of components are generated (again using LOOCV), as seen in Figure 5.3. RMSEP is defined as $\sqrt{\frac{1}{n} \sum_{i=1}^{n} (y_i - \hat{y}_i)^2}$, and is a metric which indicates how well the true target concentration (y_i) is predicted ($\hat{y}_i$) using n components.
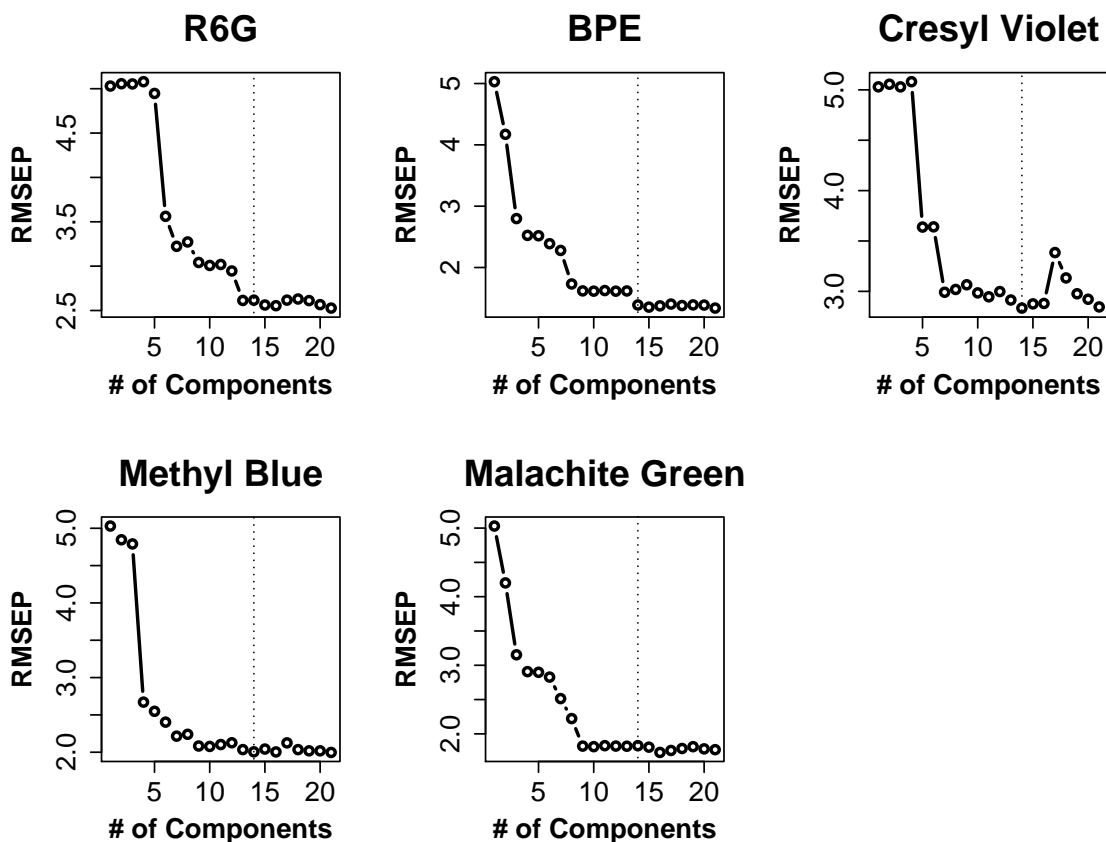
Figure 5.3: RMSEP vs. the number of components in a PLS model of the entire dataset (n = 155), using LOOCV. Dashed line indicates that 14 components were selected for use in further analysis.

The goal in selected how many components to use is to select enough components to yield a good fit of the data (minimum RMSEP) without *overfitting* the data. For this reason, it is better to select a local minimum rather than the absolute

minimum. As additional components are added beyond an initial local minimum, the danger is that the model is integrating variability which is unique to the training set to fit the data, and that these additional components will in fact *decrease* performance on new data sets. As indicated by the dotted line in Figure 5.3, 14 components were chosen for use in further analysis as additional components beyond 14 offer little improvement (in fact, they make the prediction of the analyte CV worse).

The raw value of the RMSEP can also serve as rough guidance as to the quality of fit. As can be seen, the RMSEP values for CV and R6G never drop below ~ 3 and ~ 2.5, respectively, which will be reflected in the poor prediction quality of these two analytes in the results.

In a PLS model the data $\boldsymbol{X}$ is modeled as the score matrix $\boldsymbol{T}$ times the loadings $\boldsymbol{P}$ [114], and as a result additional insight into the characteristics of the RMSEP plot (Figure 5.3) can be gleamed by visualizing these loadings. A plot of the loadings for the first 4 components is contained in Figure 5.4. In Figure 5.3, one can see that the first three components reduce the RMSEP of MG and BPE substantially, and this is reflected by the fact that the loadings of the first three components in Figure 5.4 resemble combinations of the spectra of these two analytes.

All analysis was implemented in R [115], an open source language for statistical computing, taking advantage of the pls package [116] for PLS regression and the btw package for background subtraction [117].
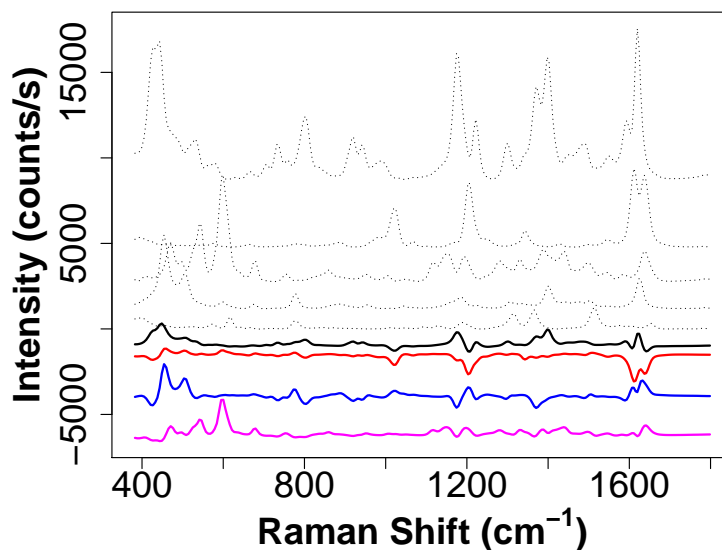
Figure 5.4: Plot of loadings of the first four components (from #4 in
magenta at bottom to #1 in middle in black). Pure spectra of the 5
analytes used in this analysis are show in the top half of the plot in
light gray. The loadings plot offeres a visualization of the
characteristics the PLS model.

5.3 Results

5.3.1 PLS analysis of highly multiplex SERS data

To demonstrate the potential for increasing the multiplexing capabilities of
a SERS detection system through multivariate statistical analysis, we conducted a
PLS analysis of 5 SERS analytes. Samples were analyzed which contained each of
the 31 possible combinations of analytes. This allowed for generation of a thorough
model which could account for some of the complex variability which arises in highly
multiplexed samples, in which the height of the peaks can no longer be directly
correlated to analyte concentration. The predicted concentrations of analytes (using
LOOCV and 14 PLS components) are displayed in Figure 5.5.

As seen in Figure 5.2, the highly multiplex data does not represent a linear
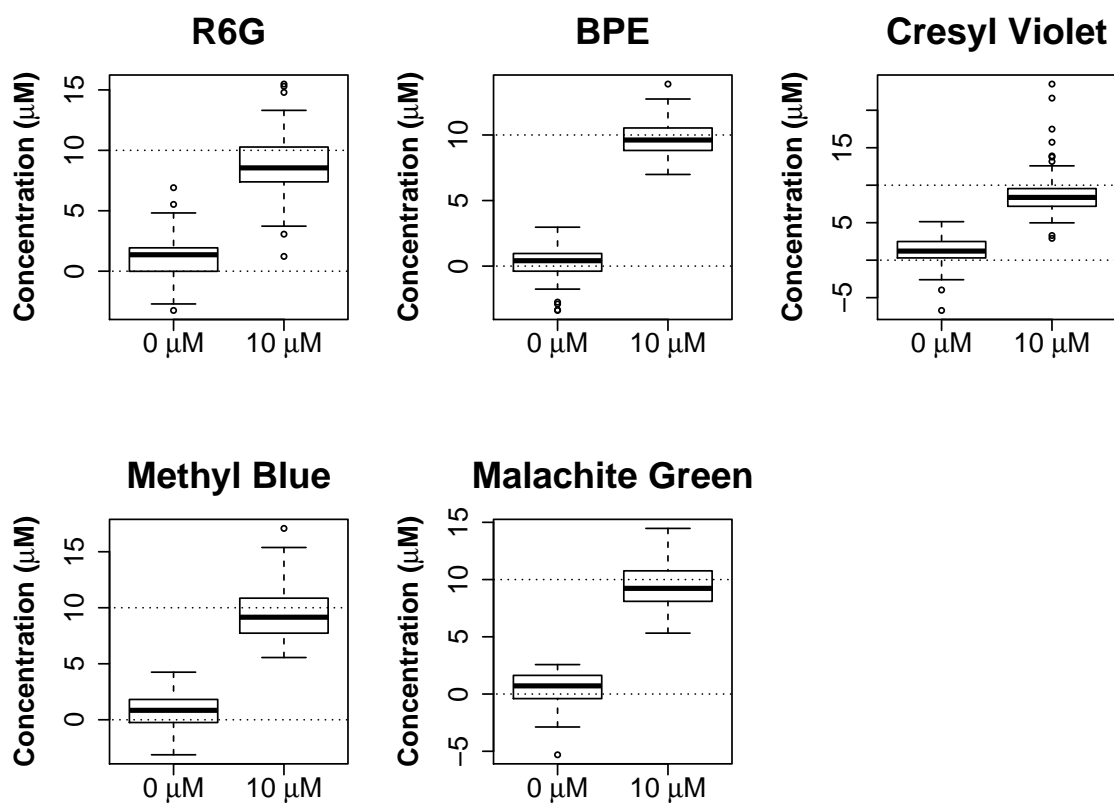
Figure 5.5: PLS cross validated predictions 14 comps

combination of the underlying spectra. This presents a formidable challenge in separating them out; nevertheless, the PLS model is able to account for a substantial degree of this variability due to complex analyte interactions and generates reasonable predictions of analyte concentration, significantly outperforming a naked eye analysis. For strongly binding molecules with large Raman cross-sections, such as BPE and MG, the model is able to offer fairly accurate predictions of actual concentration. However for weaker molecules such as R6G, the model has difficulty distinguishing between presence and absence of the target.

In addition to the variability is caused by differing affinity for the metal surface and different Raman cross-sections, there is also some variability due to the SERS substrate itself as well as the varying degrees of wicking upon sample application (different analytes have different affinities for the cellulose substrate support). The first types of variability can be accounted for by the PLS model with no user input, but in a labeled assay such as that presented in Chapter 4, this issue is further mitigated as typical dyes used to label DNA all have similar affinities for the metal nanoparticles and can be selected to have similar Raman cross sections. Addressing the latter sources of variability requires changes to experimental design.

Treating this data as data from an on/off response, as seen in the labeled assay in Chapter 4, we can define a threshold of 5μM and evaluate the occurrence of false negatives and false positives, as shown in Figure 5.6. For an assay with an on/off response, this assay would perform suitably for BPE, MB and MG, which some false positives and negatives for R6G and CV.

To further investigate the causes of the erroneous predictions, we specifically
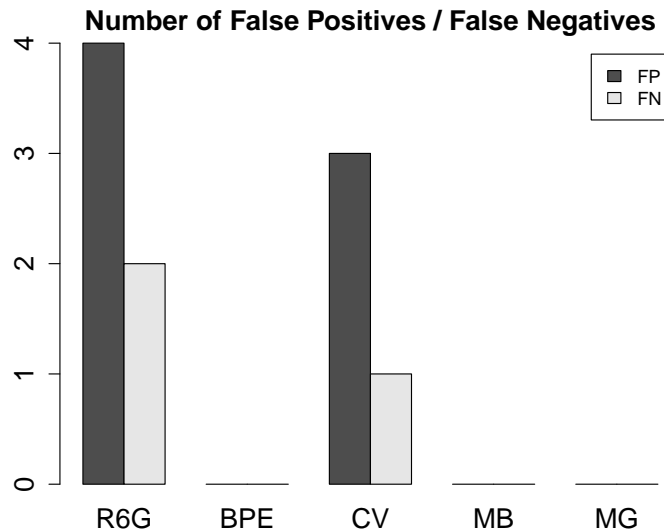
Figure 5.6: Bar chart of false positives and negatives found in this study (total n = 155), with a threshold of 5 μM used to partition between "positive" and "negative".

look at most erroneous false positive prediction for R6G (a prediction of 6.9 μM). Figure 5.7 shows the spectrum for this false positive in red (the inset shows the corresponding datapoint from the PLS LOOCV predictions for R6G). For reference, the other 4 spectra from the same analyte mixture (BPE, CV and MG) are shown in dotted lines, and the spectrum for pure R6G is shown in black at the bottom. By viewing the data in the manner, it is easy to see that the model failed due to bad data, rather than having failed in fitting. The data that generated the false positive (red trace) can be seen diverging from the other 4 spectra from the same sample (dotted lines) at a number of points, particularly around 450 cm^{-1} and 1400 cm^{-1}.
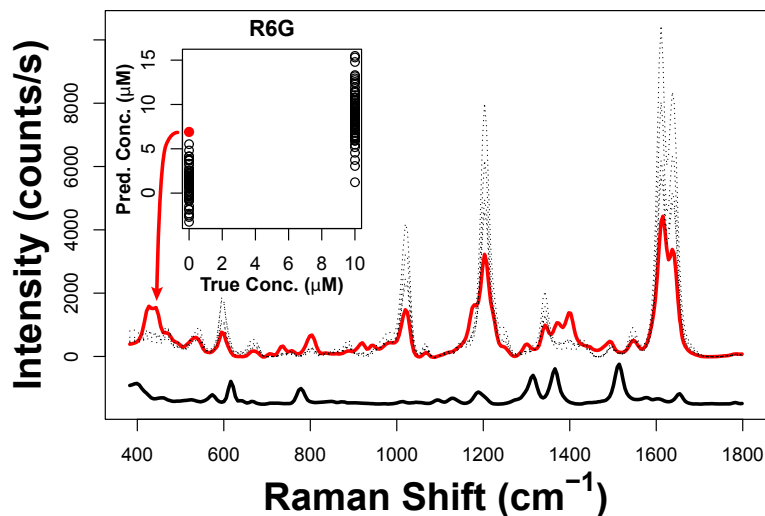
Figure 5.7: Plot of the spectrum corresponding to the most erroneous false positive identified during leave-one-out cross validation of the PLS model (in red). Inset shows a scatter plot of all predicted vs. true concentrations for R6G. For reference, the 4 other spectra from the same mixture of analytes are shown in dotted black lines and a pure R6G spectrum is shown in black at the bottom. Intuitively, one can see that poor data quality caused this bad prediction.

5.3.2 Spatial averaging to improve quality of PLS prediction

While the performance of the PLS model is reasonable under highly multiplexed conditions, it is insufficient for a diagnostic assay such as that presented in Chapter 4. Two promising avenues of improvement exist. On the experimental design side, the inherent analyte variability can be addressed by choosing labels with similar affinities for the substrate and similar Raman cross sections, and would substantially improve model quality. On the data collection side, significant improvements can be realized by reducing the spatial variability seen in these substrates. The simplest way to do this is by rastering over a moderately sized area (a few mm) at detection time, a capability offered by many commercial spectroscopy systems. In the absence of a rastering system, the same effect can be achieved by collecting

spectra at a few locations and averaging them.

To investigate the potential improvements offered by optimizing data collection methodologies, we studied the effect of spatially averaging spectra. Since the dataset consists of 5 spectra for each of the 31 different combinations of analytes, we iteratively withheld the 5 spectra corresponding to one mixture of analytes and generated a PLS model using the remaining $30 \times 5 = 155$ spectra, then used this model to predict the concentration of the *average* of the 5 withheld spectra. By iterating over the 31 combinations of analytes this offered the opportunity to predict the presence of 10 μM of each sample 16 times, and 0 μM 15 times.

The results of the PLS predictions of spatially averaged spectra are shown in Figure 5.8. It is immediately apparent that the quality of the predictions have improved dramatically. For all of the analytes, the predictions fall fairly tightly around the true concentrations (indicated by the dashed lines), even in the case of the challenging 5 way multiplexed spectrum which is impossible to visually evaluate (black line, Figure 5.2). For an on/off diagnostic assay such as that seen in Chapter 4, this technique shows the potential to offer a consistently accurate diagnosis with no false positives or negatives.

5.4   Conclusion

SERS is frequently touted as a detection mechanism enabling evaluation of highly multiplex samples, however the vast majority of SERS publications present results using only one or a few targets and take the ability to scale to highly mul-
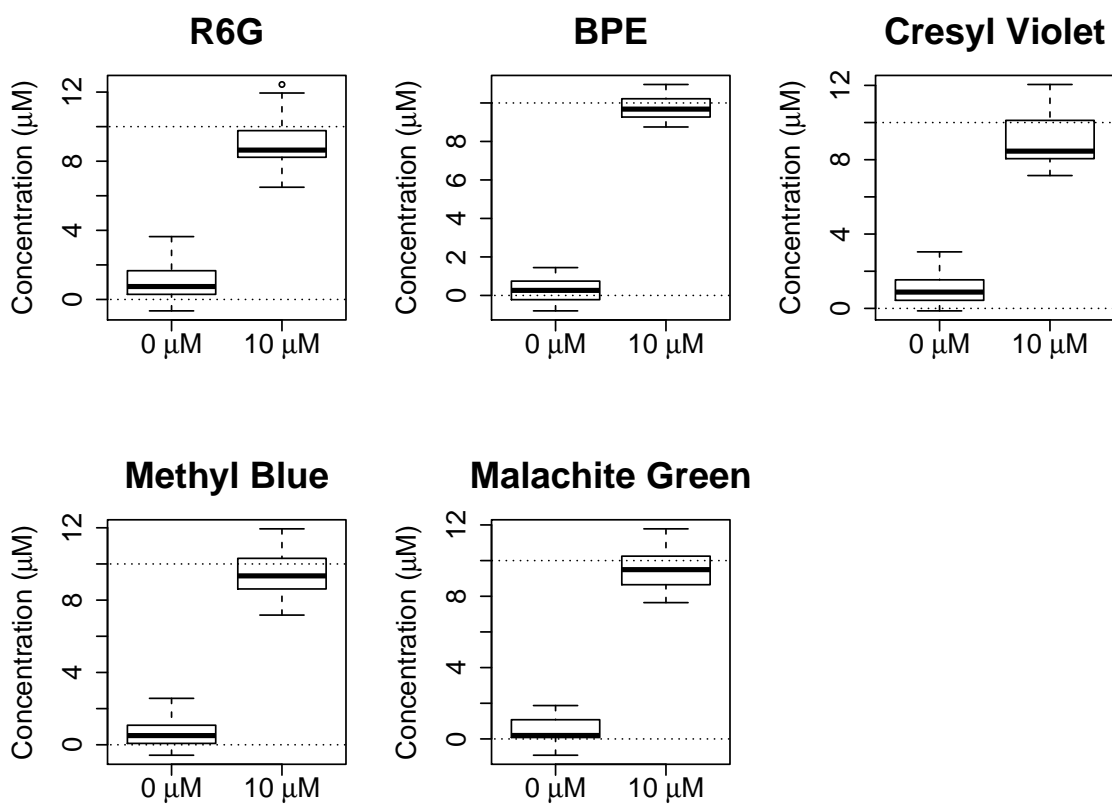
Figure 5.8: In this figure, the model was trained on a subset of data leaving out the 5 data poitns corresponding to one possibility (e.g. duplex of M.G. and C.V.). This model was then validated on the *average* of the 5 withheld spectra. The process was iterated until this had been performed for all 31 possible combinations of the 5 analytes. The improvement in results is dramatic, and shows the promise of a rastered measurement vs. the static measurements used in this study.

tiplex samples on faith. We have demonstrated the feasibility of using statistical multivariate techniques to enable evaluation of highly convoluted SERS spectra, extracting relatively accurate estimates of analyte concentration despite the fact that these convoluted spectra are dramatically different from linear combination of the underlying spectra. Through a simple but robust asymmetric least-squares baseline subtraction, the unwanted variability due to the signal background is eliminated. We demonstrate how to choose an appropriate number of components for a PLS model, and then apply this to predict concentrations using leave-one-out cross-validation of a data-set containing 155 samples. While this generates reasonable predictions of analyte concentration, it does not offer perfect discrimination. We then demonstrate that an improved prediction can be achieved by spatially averaging spectra before analysis, yielding tight predictions of analyte concentration even for the most challenging $5\times$ multiplex case. This study indicates that it is possible to use SERS as a detection mechanism for highly multiplexed labeled assays and obtain an accurate and reliable diagnosis.

Chapter 6

Conclusion

6.1 Summary of findings

In this work we investigated the use and optimization of ink-jet printed surface enhanced Raman spectroscopy (SERS) sensors for chemical and bio-molecule detection. Using cellulose as the SERS substrate support matrix offers unique capabilities, including a pump-free microfluidic system which can perform chromatographic separation and concentration of analytes *within* the substrate itself. The capabilities of the substrate to simultaneously separate and concentrate analytes were leveraged to enable multiplexed detection of DNA targets from a PCR reaction. Multiplexing considerations and potential were examined.

In Chapter 3, detection of a number of chemical analytes was performed in a variety of assay formats. The analyte-dependent effect of the membrane support material (unmodified cellulose versus nitrocellulose) on sensor performance was examined. We demonstrated the quantitative potential and excellent enhancement factor of the printed SERS sensors using BPE as a model analyte. It was found that the number of print cycles has a biphasic effect on SERS enhancement, initially improving rapidly with increasing ink volume before reaching a peak and slowly declining.

A number of application examples were given using the optimized substrates.

To demonstrate the potential for quantitative chemical detection, we applied BPE in bulk to the sensor and found a very tight fit to the Langmuir isotherm ($R^2 = 0.99$). To explore the potential for leveraging the paper-fluidic properties of the substrate to enhance the signal, we applied BPE to the sensor in bulk and then performed a lateral flow concentration, which boosted the signal by an order of magnitude. We also demonstrated the detection of a fungicide in water using a dipstick, showing a concentration effect with a longer dip. Finally, we used the SERS sensors as a surface swab, showing excellent SERS detection of the fungicide Thiram on a surface at the 10's of nanograms level.

In Chapter 4 we introduced a novel DNA detection assay, in which the sensitivity and multiplexing capabilities of SERS are combined with DNA amplification through polymerase chain reaction (PCR). Previous efforts to combine SERS with PCR have exhibited a variety of drawbacks, including low signal contrast, complex sample processing steps and inverse signal responses. We demonstrated a new assay in which Raman reporter probes (RRPs) on DNA are placed in a PCR reaction, where they are hydrolyzed *if the target is present.* Then a simple dipstick separation can be performed using an ink-jet printed SERS device; if the RRPs are hydrolyzed, indicating target presence, they are soluble and will migrate to the detection zone, while if no target was present the RRPs are insoluble and will not be detected.

We developed a duplex PCR assay as a test case, in which we targeted the Methicillin-resistant *Staphylococcus aureus* (MRSA) genes *mecA* and *femB*, two genes which confer antibiotic resistance on MRSA. After identifying optimal primer and probe sequences and reaction conditions using traditional fluorescence-based

PCR, we then used this assay to perform duplex detection of *mecA* and *femB* using SERS. The basic concepts of PCR are conserved in our new assay, making this a drop-in replacement to enable highly multiplex detection of targets in existing probe-based PCR assays.

In Chapter 5, we explored extending SERS assays which employ RRPs to high levels of multiplexing. While the potential of SERS as a highly multiplexable detection modality is consistently taken for granted in the literature, it is almost never addressed experimentally. As the potential of the assay in Chapter 4 is only realized when performing highly multiplexed detection, we explored the multiplex detection of mixtures containing combinations of 5 different Raman reporters. A naked eye analysis of the highly multiplex data was found to be impossible since the spectra do not represent the sort of linear combinations of the underlying constituents which one might have expected. Using partial least-squares regression (PLS) we demonstrate the differentiation of these samples with a high degree of accuracy, and further improve this accuracy by spatially averaging the signals within a single substrate. Using this improved method, the data could be thresholded at the level of 50% signal yielding no false negatives or false positives.

6.2   Contributions to the field and potential impact

As the SERS field has developed over the past 40 years, researchers have persistently sought to generate substrates enabling high degrees of enhancement in a consistent and reliable manner. While there are numerous successes, in some cases

enabling single-molecule detection, almost all of the substrates meeting these criteria require clean-room fabrication or other highly complex processing regimes. We have built on the work of Yu et al. [11, 118] in developing a paper SERS platform which is suitable for reliable analysis. We reported the large enhancement (10^6 or more) and low inter-substrate variability of these inexpensive substrates, the opportunity to tune the support matrix depending on the analyte of interest and also reported examples of numerous chemical detection applications.

Using these substrates, we developed a novel assay which combines the concept of hydrolysis PCR probes with paper SERS devices. Leveraging the wicking and chromatographic capabilities of the SERS substrates, we enabled discrimination and SERS detection of multiple DNA targets within a single dipstick. By performing the discrimination *within* the SERS device itself, the complex sample processing steps required by other SERS DNA detection techniques were avoided.

Finally, we performed a detailed PLS chemometric analysis of 5-plex SERS data, and investigated the practical concerns and performance of such an assay. While the well known variability of SERS resulted in imperfect discrimination, we found that by averaging over a larger area of the substrate this issue could be mitigated, yielding very good predictive capability which would translate into no false positives or negatives. This technique can be generally applied to SERS assays and specifically to the SERS-PCR assay we developed to enable highly multiplex screening for infectious diseases within a single sample and SERS device.

6.3 Future work

In this work, we investigated the potential of the paper-SERS platform for chemical and biological analysis. We believe that the SERS-PCR assay presented here could serve as a foundation for a simple, highly multiplexed assay. However, additional research is needed. We envision three main areas of further study: sample collection and preparation, SERS-PCR assay format and amplification equipment.

The current implementation of the assay was performed using purified DNA as the sample matrix. With real-world infectious disease samples, first the cells must be lysed to free the DNA and then the DNA is purified. All of the commonly used DNA purification schemes (e.g. phase separation, solid phase extraction) require substantial manual labor and most require expensive equipment. A study of performing PCR directly on raw lysate should be undertaken, to determine the effect on reliability of the assay. While PCR is not commonly performed on raw lysate, it is possible to do so with good results [119]. As an alternative, it may be possible to develop a simple wound swab with integrated lysis enzymes, which could be used in a dipstick fashion to purify DNA within the swab following sample collection.

Another area of future investigation is the format of the SERS-PCR assay itself. Currently, samples are manually applied to the SERS dipsticks, before being dried, run and measured. While this is suitable in a research lab setting, a more robust assay design is needed for real-world use. Designing a cartridge system which holds the SERS dipstick in place and aids in sample application would allow the assay to be used with substantially less training.

Finally, the amplification equipment used in this study is far too expensive to be suitable for a low resource assay. We envision that this SERS-based assay, in combination with a single-reaction low-cost thermocycler, could serve as the basis for a simple on-site assay which screens for a panel of infectious diseases.

Bibliography

[1] Kurt Varmuza and Peter Filzmoser. *Introduction to Multivariate Statistical Analysis in Chemometrics*. CRC Press, 2008.

[2] Jeffrey M. McMahon, Shuzhou Li, Logan K. Ausman, and George C. Schatz. Modeling the Effect of Small Gaps in Surface-Enhanced Raman Spectroscopy. *The Journal of Physical Chemistry C*, 116(2):1627–1637, 2012.

[3] David G Ginzinger. Gene quantification using real-time quantitative PCR: An emerging technology hits the mainstream. *Experimental Hematology*, 30(6):503–512, 2002.

[4] YunWei Charles Cao, Rongchao Jin, and Chad A. Mirkin. Nanoparticles with Raman Spectroscopic Fingerprints for DNA and RNA Detection. *Science*, 297(5586):1536 –1540, 2002.

[5] Eric P. Hoppmann, Wei W. Yu, and Ian M. White. Inkjet-printed fluidic paper devices for chemical and biological analytics using surface enhanced Raman spectroscopy. *IEEE Journal of Selected Topics in Quantum Electronics*, 2014 DOI: 10.1109/JSTQE.2013.2286076.

[6] Centers for Disease Control. National Ambulatory Medical Care Survey: 2009, 2009.

[7] Yi-Wei Tang, Gary W Procop, and David H Persing. Molecular diagnostics of infectious diseases. *Clinical chemistry*, 43(11):2021–2038, 1997.

[8] Marie Louie, Lisa Louie, and Andrew E. Simor. The role of DNA amplification technology in the diagnosis of infectious diseases. *CMAJ: Canadian Medical Association Journal*, 163(3):301–309, 2000.

[9] Shuming Nie and Steven R. Emory. Probing Single Molecules and Single Nanoparticles by Surface-Enhanced Raman Scattering. *Science*, 275(5303):1102–1106, 1997.

[10] Katrin Kneipp, Yang Wang, Harald Kneipp, Lev T. Perelman, Irving Itzkan, Ramachandra R. Dasari, and Michael S. Feld. Single Molecule Detection Using Surface-Enhanced Raman Scattering (SERS). *Physical Review Letters*, 78(9):1667–1670, 1997.

[11] Wei W. Yu and Ian M. White. Inkjet Printed Surface Enhanced Raman Spectroscopy Array on Cellulose Paper. *Analytical Chemistry*, 82(23):9626–9630, 2010.

[12] Karen Faulds, W. Ewen Smith, and Duncan Graham. Evaluation of Surface-Enhanced Resonance Raman Scattering for Quantitative DNA Analysis. *Analytical Chemistry*, 76(2):412–417, 2004.

[13] M. Fleischmann, P.J. Hendra, and A.J. McQuillan. Raman spectra of pyridine adsorbed at a silver electrode. *Chemical Physics Letters*, 26(2):163–166, 1974.

[14] M. Grant Albrecht and J. Alan Creighton. Anomalously intense Raman spectra of pyridine at a silver electrode. *Journal of the American Chemical Society*, 99(15):5215–5217, 1977.

[15] David L. Jeanmaire and Richard P. Van Duyne. Surface raman spectroelectrochemistry: Part I. Heterocyclic, aromatic, and aliphatic amines adsorbed on the anodized silver electrode. *Journal of Electroanalytical Chemistry and Interfacial Electrochemistry*, 84(1):1–20, 1977.

[16] M. Moskovits. Surface roughness and the enhanced intensity of Raman scattering by molecules adsorbed on metals. *The Journal of Chemical Physics*, 69:4159, 1978.

[17] Martin Moskovits. Surface-enhanced spectroscopy. *Reviews of Modern Physics*, 57(3):783–826, 1985.

[18] Katrin Kneipp, Harald Kneipp, Irving Itzkan, Ramachandra R Dasari, and Michael S Feld. Ultrasensitive Chemical Analysis by Raman Spectroscopy. *Chemical Reviews*, 99(10):2957–2976, 1999.

[19] Amy M Michaels, M Nirmal, and LE Brus. Surface Enhanced Raman Spectroscopy of Individual Rhodamine 6G Molecules on Large Ag Nanocrystals. *Journal of the American Chemical Society*, 121(43):9932–9939, 1999.

[20] Katrin Kneipp, Harald Kneipp, V. Bhaskaran Kartha, Ramasamy Manoharan, Geurt Deinum, Irving Itzkan, Ramachandra R. Dasari, and Michael S. Feld. Detection and identification of a single DNA base molecule using surface-enhanced Raman scattering (SERS). *Physical Review E*, 57(6):R6281–R6284, 1998.

[21] Michael J Weaver, Shouzhong Zou, and Ho Yeung H Chan. Peer Reviewed: The New Interfacial Ubiquity of Surface-Enhanced Raman Spectroscopy. *Analytical Chemistry*, 72(1):38A–47A, 2000.

[22] Alan Campion and Patanjali Kambhampati. Surface-enhanced Raman scattering. *Chemical Society Reviews*, 27(4):241–250, 1998.

[23] B. J. Kennedy, S. Spaeth, M. Dickey, and K. T. Carron. Determination of the Distance Dependence and Experimental Effects for Modified SERS Substrates Based on Self-Assembled Monolayers Formed Using Alkanethiols. *The Journal of Physical Chemistry B*, 103(18):3640–3646, 1999.

[24] D. A. Weitz, S. Garoff, J. I. Gersten, and Abraham Nitzan. The enhancement of Raman scattering, resonance Raman scattering, and fluorescence from molecules adsorbed on a rough silver surface. *The Journal of Chemical Physics*, 78(9):5324, 1983.

[25] Peter Hildebrandt and Manfred Stockburger. Surface-enhanced resonance Raman spectroscopy of Rhodamine 6G adsorbed on colloidal silver. *The Journal of Physical Chemistry*, 88(24):5935–5944, 1984.

[26] AA Stacy and RP Van Duyne. Surface enhanced raman and resonance raman spectroscopy in a non-aqueous electrochemical environment: tris (2,2′-bipyridine) ruthenium (II) adsorbed on silver from acetonitrile. *Chemical Physics Letters*, 102(4):365–370, 1983.

[27] O. Siiman, A. Lepp, and M. Kerker. Combined surface-enhanced and resonance-Raman scattering from the aspartic acid derivative of methyl orange on colloidal silver. *The Journal of Physical Chemistry*, 87(26):5319–5325, 1983.

[28] Duncan Graham and Karen Faulds. Quantitative SERRS for DNA sequence analysis. *Chemical Society Reviews*, 37(5):1042–1051, 2008.

[29] Sumeet Mahajan, James Richardson, Tom Brown, and Philip N. Bartlett. SERS-Melting: A New Method for Discriminating Mutations in DNA Sequences. *Journal of the American Chemical Society*, 130(46):15589–15601, 2008.

[30] Zhong-Qun Tian, Bin Ren, and De-Yin Wu. Surface-Enhanced Raman Scattering: From Noble to Transition Metals and from Rough Surfaces to Ordered Nanostructures. *The Journal of Physical Chemistry B*, 106(37):9463–9483, 2002.

[31] Samuel L. Kleinman, Renee R. Frontiera, Anne-Isabelle Henry, Jon A. Dieringer, and Richard P. Van Duyne. Creating, characterizing, and controlling chemistry with SERS hot spots. *Physical Chemistry Chemical Physics*, 15(1):21–36, 2012.

[32] Weiyang Li, Pedro H. C. Camargo, Xianmao Lu, and Younan Xia. Dimers of Silver Nanospheres: Facile Synthesis and Their Use as Hot Spots for Surface-Enhanced Raman Scattering. *Nano Letters*, 9(1):485–490, 2009.

[33] Stephen B. Chaney, Saratchandra Shanmukh, Richard A. Dluhy, and Y.-P. Zhao. Aligned silver nanorod arrays produce high sensitivity surface-enhanced Raman spectroscopy substrates. *Applied Physics Letters*, 87(3):031908–03190, 2005.

[34] Hsiangkuo Yuan, Yang Liu, Andrew M. Fales, You Leo Li, Jesse Liu, and Tuan Vo-Dinh. Quantitative Surface-Enhanced Resonant Raman Scattering Multiplexing of Biocompatible Gold Nanostars for in Vitro and ex Vivo Detection. *Analytical Chemistry*, 85(1):208–212, 2013.

[35] Traci R. Jensen, Michelle Duval Malinsky, Christy L. Haynes, and Richard P. Van Duyne. Nanosphere Lithography: Tunable Localized Surface Plasmon

Resonance Spectra of Silver Nanoparticles. *The Journal of Physical Chemistry B*, 104(45):10549–10556, 2000.

[36] Hyungsoon Im, Kyle C. Bantz, Nathan C. Lindquist, Christy L. Haynes, and Sang-Hyun Oh. Vertically Oriented Sub-10-nm Plasmonic Nanogap Arrays. *Nano Letters*, 10(6):2231–2236, 2010.

[37] Xuegong Deng, Gary B. Braun, Sheng Liu, Paul F. Sciortino, Bob Koefer, Thomas Tombler, and Martin Moskovits. Single-Order, Subwavelength Resonant Nanograting as a Uniformly Hot Substrate for Surface-Enhanced Raman Spectroscopy. *Nano Letters*, 10(5):1780–1786, 2010.

[38] R. Griffith Freeman, Katherine C. Grabar, Keith J. Allison, Robin M. Bright, Jennifer A. Davis, Andrea P. Guthrie, Michael B. Hommer, Michael A. Jackson, Patrick C. Smith, Daniel G. Walter, and Michael J. Natan. Self-Assembled Metal Colloid Monolayers: An Approach to SERS Substrates. *Science*, 267(5204):1629–1632, 1995.

[39] Christopher J. Orendorff, Anand Gole, Tapan K. Sau, and Catherine J. Murphy. Surface-Enhanced Raman Spectroscopy of Self-Assembled Monolayers: Sandwich Architecture and Nanoparticle Shape Dependence. *Analytical Chemistry*, 77(10):3261–3266, 2005.

[40] Hui Wang, Carly S. Levin, and Naomi J. Halas. Nanosphere Arrays with Controlled Sub-10-nm Gaps as Surface-Enhanced Raman Spectroscopy Substrates. *Journal of the American Chemical Society*, 127(43):14992–14993, 2005.

[41] Luis M. Liz-MarzÃąn. Tailoring Surface Plasmons through the Morphology and Assembly of Metal Nanoparticles. *Langmuir*, 22(1):32–41, 2006.

[42] Daniel M. Kuncicky, Brian G. Prevo, and Orlin D. Velev. Controlled assembly of SERS substrates templated by colloidal crystal films. *Journal of Materials Chemistry*, 16(13):1207–1211, 2006.

[43] Hye Young Jung, Yong-Kyun Park, Sungho Park, and Seong Kyu Kim. Surface enhanced Raman scattering from layered assemblies of close-packed gold nanoparticles. *Analytica Chimica Acta*, 602(2):236–243, 2007.

[44] V. Liberman, C. Yilmaz, T. M. Bloomstein, S. Somu, Y. Echegoyen, A. Busnaina, S. G. Cann, K. E. Krohn, M. F. Marchant, and M. Rothschild. A Nanoparticle Convective Directed Assembly Process for the Fabrication of Periodic Surface Enhanced Raman Spectroscopy Substrates. *Advanced Materials*, 22(38):4298–4302, 2010.

[45] Tuan Vo-Dinh, M. Y. K. Hiromoto, G. M. Begun, and R. L. Moody. Surface-enhanced Raman spectrometry for trace organic analysis. *Analytical Chemistry*, 56(9):1667–1670, 1984.

[46] Tuan Vo-Dinh, Mayo Uziel, and Alan L. Morrison. Surface-enhanced Raman analysis of benzo [a] pyrene-DNA adducts on silver-coated cellulose substrates. *Applied spectroscopy*, 41(4):605–610, 1987.

[47] Alain Berthod, J. J. Laserna, and J. D. Winefordner. Analysis by surface enhanced Raman spectroscopy on silver hydrosols and silver coated filter papers. *Journal of Pharmaceutical and Biomedical Analysis*, 6(6):599–608, 1988.

[48] Javier J. Laserna, Andres D. Campiglia, and J. D. Winefordner. Mixture analysis and quantitative determination of nitrogen-containing organic molecules by surface-enhanced Raman spectrometry. *Analytical chemistry*, 61(15):1697–1701, 1989.

[49] L. M. Cabalin and J. J. Laserna. Fast spatially resolved surface-enhanced Raman spectrometry on a silver coated filter paper using charge-coupled device detection. *Analytica chimica acta*, 310(2):337–345, 1995.

[50] Chang H. Lee, Mikella E. Hankus, Limei Tian, Paul M. Pellegrino, and Srikanth Singamaneni. Highly Sensitive Surface Enhanced Raman Scattering Substrates Based on Filter Paper Loaded with Plasmonic Nanostructures. *Analytical Chemistry*, 83(23):8953–8958, 2011.

[51] Ying Hui Ngo, Dan Li, George P. Simon, and Gil Garnier. Gold nanoparticle–paper as a three-dimensional surface enhanced Raman scattering substrate. *Langmuir*, 28(23):8782–8790, 2012.

[52] Dora Mehn, Carlo Morasso, Renzo Vanna, Marzia Bedoni, Davide Prosperi, and Furio Gramatica. Immobilised gold nanostars in a paper-based test system for surface-enhanced Raman spectroscopy. *Vibrational Spectroscopy*, 68:45–50, 2013.

[53] Lu-Lu Qu, Da-Wei Li, Jin-Qun Xue, Wen-Lei Zhai, John S. Fossey, and Yi-Tao Long. Batch fabrication of disposable screen printed SERS arrays. *Lab on a Chip*, 12(5):876–881, 2012.

[54] Min-Liang Cheng, Bo-Chan Tsai, and Jyisy Yang. Silver nanoparticle-treated filter paper as a highly sensitive surface-enhanced Raman scattering (SERS) substrate for detection of tyrosine in aqueous solution. *Analytica Chimica Acta*, 708(1âĂŞ2):89–96, 2011.

[55] P. C. Lee and D. Meisel. Adsorption and surface-enhanced Raman of dyes on silver and gold sols. *J. Phys. Chem.*, 86(17):3391–3395, 1982.

[56] Eric P. Hoppmann, Wei W. Yu, and Ian M. White. Highly sensitive and flexible inkjet printed SERS sensors on paper. *Methods*, 63(3):219–224, 2013.

[57] T L Bannerman, G A Hancock, F C Tenover, and J M Miller. Pulsed-field gel electrophoresis as a replacement for bacteriophage typing of Staphylococcus aureus. *Journal of Clinical Microbiology*, 33(3):551–555, 1995.

[58] Mark C. Enright, D. Ashley Robinson, Gaynor Randle, Edward J. Feil, Hajo Grundmann, and Brian G. Spratt. The evolutionary history of methicillin-resistant *Staphylococcus aureus* (MRSA). *Proceedings of the National Academy of Sciences*, 99(11):7687 –7692, 2002.

[59] Eva Engvall and Peter Perlmann. Enzyme-Linked Immunosorbent Assay, Elisa III. Quantitation of Specific Antibodies by Enzyme-Labeled Anti-Immunoglobulin in Antigen-Coated Tubes. *The Journal of Immunology*, 109(1):129–135, 1972.

[60] K.A. Wetterstrand. NA Sequencing Costs: Data from the NHGRI Genome Sequencing Program (GSP), 2013.

[61] Alec J. Jeffreys, Victoria Wilson, and Swee Lay Thein. Hypervariable 'mini-isatellite' regions in human DNA. *Nature*, 314(6006):67–73, 1985.

[62] G. Prevost, B. Jaulhac, and Y. Piemont. DNA fingerprinting by pulsed-field gel electrophoresis is more effective than ribotyping in distinguishing among methicillin-resistant Staphylococcus aureus isolates. *Journal of clinical microbiology*, 30(4):967–973, 1992.

[63] Fred C. Tenover, Robert D. Arbeit, Richard V. Goering, Patricia A. Mickelsen, Barbara E. Murray, David H. Persing, and Bala Swaminathan. Interpreting chromosomal DNA restriction patterns produced by pulsed-field gel electrophoresis: criteria for bacterial strain typing. *Journal of clinical microbiology*, 33(9):2233, 1995.

[64] Ian M. Mackay, Katherine E. Arden, and Andreas Nitsche. Real-time PCR in virology. *Nucleic Acids Research*, 30(6):1292 –1305, 2002.

[65] Henry A. Erlich, David Gelfand, and John J. Sninsky. Recent Advances in the Polymerase Chain Reaction. *Science*, 252(5013):1643–1651, 1991.

[66] C. A. Heid, J. Stevens, K. J. Livak, and P. M. Williams. Real time quantitative PCR. *Genome Research*, 6(10):986–994, 1996.

[67] Elfath M. Elnifro, Ahmed M. Ashshi, Robert J. Cooper, and Paul E. Klapper. Multiplex PCR: Optimization and Application in Diagnostic Virology. *Clinical Microbiology Reviews*, 13(4):559–570, 2000.

[68] Carl T. Wittwer, Mark G. Herrmann, Cameron N. Gundry, and Kojo S.J. Elenitoba-Johnson. Real-Time Multiplex PCR Assays. *Methods*, 25(4):430–442, 2001.

[69] P M Holland, R D Abramson, R. Watson, and D H Gelfand. Detection of Specific Polymerase Chain Reaction Product by Utilizing the 5'—3' Exonuclease Activity of Thermus Aquaticus DNA Polymerase. *Proceedings of the National Academy of Sciences*, 88(16):7276–7280, 1991.

[70] I. S. Patel, W. R. Premasiri, D. T. Moir, and L. D. Ziegler. Barcoding bacterial cells: a SERS-based methodology for pathogen identification. *Journal of Raman Spectroscopy*, 39(11):1660–1672, 2008.

[71] Desiree S. Grubisha, Robert J. Lipert, Hye-Young Park, Jeremy Driskell, and Marc D. Porter. Femtomolar Detection of Prostate-Specific Antigen:âĹ An Immunoassay Based on Surface-Enhanced Raman Scattering and Immunogold Labels. *Analytical Chemistry*, 75(21):5936–5943, 2003.

[72] Xiao X. Han, Bing Zhao, and Yukihiro Ozaki. Surface-enhanced Raman scattering for protein detection. *Analytical and Bioanalytical Chemistry*, 394(7):1719–1727, 2009.

[73] Yun Suk Huh, Aram J Chung, and David Erickson. Surface enhanced Raman spectroscopy and its application to molecular and cellular analysis. *Microfluidics and nanofluidics*, 6(3):285–297, 2009.

[74] J. D. Driskell, Y. Zhu, C. D. Kirkwood, Y. Zhao, R. A. Dluhy, and R. A. Tripp. Rapid and sensitive detection of rotavirus molecular signatures using surface enhanced Raman spectroscopy. *PloS one*, 5(4):e10222, 2010.

[75] Narayana R. Isola, David L. Stokes, and Tuan Vo-Dinh. Surface-Enhanced Raman Gene Probe for HIV Detection. *Analytical Chemistry*, 70(7):1352–1356, 1998.

[76] Karen Faulds, W. Ewen Smith, and Duncan Graham. Evaluation of Surface-Enhanced Resonance Raman Scattering for Quantitative DNA Analysis. *Anal. Chem.*, 76(2):412–417, 2003.

[77] William E. Doering and Shuming Nie. Spectroscopic Tags Using Dye-Embedded Nanoparticles and Surface-Enhanced Raman Scattering. *Analytical Chemistry*, 75(22):6171–6176, 2003.

[78] Ximei Qian, Xiang-Hong Peng, Dominic O. Ansari, Qiqin Yin-Goen, Georgia Z. Chen, Dong M. Shin, Lily Yang, Andrew N. Young, May D. Wang, and Shuming Nie. In vivo tumor targeting and spectroscopic detection with surface-enhanced Raman nanoparticle tags. *Nature Biotechnology*, 26(1):83–90, 2008.

[79] Duncan Graham, Benjamin J. Mallinder, David Whitcombe, Nigel D. Watson, and W. Ewen Smith. Simple Multiplex Genotyping by Surface-Enhanced Resonance Raman Scattering. *Analytical Chemistry*, 74(5):1069–1074, 2002.

[80] Danny van Lierop, Karen Faulds, and Duncan Graham. Separation Free DNA Detection Using Surface Enhanced Raman Scattering. *Anal. Chem.*, 83(15):5817–5821, 2011.

[81] Musundi B. Wabuyele and Tuan Vo-Dinh. Detection of Human Immunodeficiency Virus Type 1 DNA Sequence Using Plasmonics Nanoprobes. *Anal. Chem.*, 77(23):7810–7815, 2005.

[82] Alexandra MacAskill, David Crawford, Duncan Graham, and Karen Faulds. DNA Sequence Detection Using Surface-Enhanced Resonance Raman Spectroscopy in a Homogeneous Multiplexed Assay. *Analytical Chemistry*, 81(19):8134–8140, 2009.

[83] Danny van Lierop, Iain A. Larmour, Karen Faulds, and Duncan Graham. SERS Primers and Their Mode of Action for Pathogen DNA Detection. *Analytical Chemistry*, 85(3):1408–1414, 2013.

[84] Karen Faulds, Fiona McKenzie, W. Ewen Smith, and Duncan Graham. Quantitative Simultaneous Multianalyte Detection of DNA by Dual-Wavelength Surface-Enhanced Resonance Raman Scattering. *Angewandte Chemie International Edition*, 46(11):1829–1831, 2007.

[85] Jennifer A. Dougan and Karen Faulds. Surface enhanced Raman scattering for multiplexed detection. *Analyst*, 137(3):545–554, 2012.

[86] Wei W. Yu and Ian M. White. Chromatographic separation and detection of target analytes from complex samples using inkjet printed SERS substrates. *Analyst*, 138(13):3679–3686, 2013.

[87] Karen L. Norrod, Leo M. Sudnik, David Rousell, and Kathy L. Rowlen. Quantitative Comparison of Five SERS Substrates: Sensitivity and Limit of Detection. *Applied Spectroscopy*, 51(7):994–1001, 1997.

[88] Wei Wu, Min Hu, Fung Suong Ou, Zhiyong Li, and R. Stanley Williams. Cones fabricated by 3D nanoimprint lithography for highly sensitive surface enhanced Raman spectroscopy. *Nanotechnology*, 21(25):255502, 2010.

[89] Yongjun Liu, Jianguo Fan, Y-P. Zhao, Saratchandra Shanmukh, and Richard A. Dluhy. Angle dependent surface enhanced Raman scattering obtained from a Ag nanorod array substrate. *Applied Physics Letters*, 89(17):173134–173134, 2006.

[90] Shivaji Srivastava, Ranjana Sinha, and D. Roy. Toxicological effects of malachite green. *Aquatic Toxicology*, 66(3):319–329, 2004.

[91] Sandra J. Culp and Frederick A. Beland. Malachite Green: A Toxicological Review. *International Journal of Toxicology*, 15(3):219–238, 1996.

[92] Randall K. Saiki, David H. Gelfand, Susanne Stoffel, Stephen J. Scharf, Russell Higuchi, Glenn T. Horn, Kary B. Mullis, and Henry A. Erlich. Primer-directed enzymatic amplification of DNA with a thermostable DNA polymerase. *Science*, 239(4839):487–491, 1988.

[93] Alicia I. Hidron, Jonathan R. Edwards, Jean Patel, Teresa C. Horan, Dawn M. Sievert, Daniel A. Pollock, and Scott K. Fridkin. Antimicrobial-resistant pathogens associated with healthcare-associated infections: annual summary of data reported to the National Healthcare Safety Network at the Centers for Disease Control and Prevention, 2006-2007. *Infection Control and Hospital Epidemiology*, 29(11):996–1011, 2008.

[94] Klevens R, Morrison MA, Nadle J, and et al. Invasive methicillin-resistant *Staphylococcus aureus* infections in the United States. *JAMA, the Journal of the American Medical Association*, 298(15):1763–1771, 2007.

[95] K J Towner, D C Talbot, R Curran, C A Webster, and H Humphreys. Development and evaluation of a PCR-based immunoassay for the rapid detection of methicillin-resistant *Staphylococcus aureus*. *Journal of Medical Microbiology*, 47(7):607–613, 1998.

[96] D. Jonas, M. Speck, F. D. Daschner, and H. Grundmann. Rapid PCR-Based Identification of Methicillin-Resistant Staphylococcus aureus from Screening Swabs. *Journal of Clinical Microbiology*, 40(5):1821–1823, 2002.

[97] X. Qin, B. Bachman, P. Battles, A. Bell, C. Bess, C. Bickham, L. Chaboub, D. Chen, M. Coyle, D.R. Deiros, H. Dinh, L. Forbes, G. Fowler, L. Francisco, Q. Fu, S. Gubbala, W. Hale, Y. Han, L. Hemphill, S.K. Highlander, K. Hirani, M. Hogues, L. Jackson, A. Jakkamsetti, M. Javaid, H. Jiang, V. Korchina, C. Kovar, F. Lara, S. Lee, R. Mata, T. Mathew, C. Moen, K. Morales, M. Munidasa, L. Nazareth, R. Ngo, L. Nguyen, G. Okwuonu, F. Ongeri, S. Patil, J. Petrosino, C. Pham, P. Pham, L.-L. Pu, M. Puazo, R. Raj, J. Reid, J. Rouhana, N. Saada, Y. Shang, D. Simmons, R. Thornton, J. Warren, G. Weissenberger, J. Zhang, L. Zhang, C. Zhou, D. Zhu, D. Muzny, K. Worley, and R. Gibbs. Staphylococcus aureus subsp. aureus TCH70, whole genome shotgun sequence, 2009.

[98] Nicolas Le Novère. MELTING, computing the melting temperature of nucleic acid duplex. *Bioinformatics*, 17(12):1226 –1227, 2001.

[99] Hatim T. Allawi and John SantaLucia. Thermodynamics and NMR of Internal GÂůT Mismatches in DNA. *Biochemistry*, 36(34):10581–10594, 1997.

[100] Richard Owczarzy, Yong You, Bernardo G. Moreira, Jeffrey A. Manthey, Lingyan Huang, Mark A. Behlke, and Joseph A. Walder. Effects of Sodium Ions on DNA Duplex Oligomers: Improved Predictions of Melting Temperatures. *Biochemistry*, 43(12):3537–3554, 2004.

[101] D J Geha, J R Uhl, C A Gustaferro, and D H Persing. Multiplex PCR for identification of methicillin-resistant staphylococci in the clinical laboratory. *Journal of Clinical Microbiology*, 32(7):1768–1772, 1994.

[102] N. Kobayashi, H. Wu, K. Kojima, K. Taniguchi, S. Urasawa, N. Uehara, Y. Omizu, Y. Kishi, A. Yagihashi, and I. Kurokawa. Detection of *mecA*, *femA*, and *femB* Genes in Clinical Strains of Staphylococci Using Polymerase Chain Reaction. *Epidemiology and Infection*, 113(2):259–266, 1994.

[103] Karen Faulds, Roger Jarvis, W. Ewen Smith, Duncan Graham, and Royston Goodacre. Multiplexed detection of six labelled oligonucleotides using surface enhanced resonance Raman scattering (SERRS). *Analyst*, 133(11):1505–1512, 2008.

[104] William F. Massy. Principal Components Regression in Exploratory Statistical Research. *Journal of the American Statistical Association*, 60(309):234–256, 1965.

[105] S. Wold, A. Ruhe, H. Wold, and W. J. Dunn, III. The Collinearity Problem in Linear Regression. The Partial Least Squares (PLS) Approach to Generalized Inverses. *SIAM Journal on Scientific and Statistical Computing*, 5(3):735–743, 1984.

[106] Paul Geladi and Bruce R. Kowalski. Partial least-squares regression: a tutorial. *Analytica chimica acta*, 185:1–17, 1986.

[107] Arthur E. Hoerl and Robert W. Kennard. Ridge regression: Biased estimation for nonorthogonal problems. *Technometrics*, 12(1):55–67, 1970.

[108] Peter A. Jansson. Neural Networks: An Overview. *Analytical Chemistry*, 63(6):357A–362A, 1991.

[109] Bing Cheng and D. Michael Titterington. Neural networks: A review from a statistical perspective. *Statistical Science*, 9(1):2–30, 1994.

[110] Ildiko E. Frank and Jerome H. Friedman. A Statistical View of Some Chemometrics Regression Tools. *Technometrics*, 35(2):109–135, 1993.

[111] M. Barker and W. Rayens. Partial least squares for discrimination. *Journal of chemometrics*, 17(3):166–173, 2003.

[112] Whitney K. Newey and James L. Powell. Asymmetric Least Squares Estimation and Testing. *Econometrica*, 55(4):819–847, 1987.

[113] Paul H. C. Eilers. Parametric Time Warping. *Analytical Chemistry*, 76(2):404–411, 2004.

[114] Svante Wold, Kim Esbensen, and Paul Geladi. Principal component analysis. *Chemometrics and Intelligent Laboratory Systems*, 2(1):37–52, 1987.

[115] R Core Team. *R: A Language and Environment for Statistical Computing*. R Foundation for Statistical Computing, Vienna, Austria, 2013.

[116] Björn-Helge Mevik and Ron Wehrens. The pls package: principal component and partial least squares regression in R. *Journal of Statistical Software*, 18(2):1–24, 2007.

[117] Tom G. Bloemberg, Jan Gerretzen, Hans J.P. Wouters, Jolein Gloerich, Maurice van Dael, Hans J.C.T. Wessels, Lambert P. van den Heuvel, Paul H.C. Eilers, Lutgarde M.C. Buydens, and Ron Wehrens. Improved parametric time warping for proteomics. *Chemometrics and Intelligent Laboratory Systems*, 104(1):65–74, 2010.

[118] Wei W. Yu and Ian M. White. Inkjet-printed paper-based SERS dipsticks and swabs for trace chemical detection. *Analyst*, 138(4):1020–1025, 2013.

[119] Wl Hynes, JJ Ferretti, MS Gilmore, and RA Segarra. PCR Amplification of Streptococcal DNA Using Crude Cell Lysates. *FEMS Microbiology Letters*, 94(1):139–142, 1992.